frontiers | Frontiers in Astronomy and Space Sciences

TYPE Original Research
PUBLISHED 03 October 2023
DOI 10.3389/fspas.2023.1246978

OPEN ACCESS

EDITED BY
Milan S. Dimitrijevic,
Astronomical Observatory, Serbia

REVIEWED BY
Toshiki Saito,
National Astronomical Observatory of Japan (NAOJ), Japan
Xindi Tang,
Chinese Academy of Sciences (CAS), China

*CORRESPONDENCE
Qian Jiao,
jiaoqian@whpu.edu.cn

RECEIVED 25 June 2023
ACCEPTED 13 September 2023
PUBLISHED 03 October 2023

CITATION
Jiao Q, Gao Y, Tan Q and Gao Y (2023), Dense gas star formation efficiency and the $L'_{HCN(4-3)}/L'_{HCO^+\ (4-3)}$ ratio: insights from a statistical study of infrared bright star-forming galaxies.
Front. Astron. Space Sci. 10:1246978.
doi: 10.3389/fspas.2023.1246978

Dense gas star formation efficiency and the $L'_{HCN\,(4-3)}/L'_{HCO^+\ (4-3)}$ ratio: insights from a statistical study of infrared bright star-forming galaxies

Qian Jiao[1,2]*, Yu Gao[3,2], Qinghua Tan[2] and Yang Gao[4,2]

[1]School of Electrical and Electronic Engineering, Wuhan Polytechnic University, Wuhan, China, [2]Purple Mountain Observatory, Chinese Academy of Sciences (CAS), Nanjing, China, [3]Department of Astronomy, Xiamen University, Xiamen, Fujian, China, [4]College of Physics and Electronic Information, Dezhou University, Dezhou, China

We present a statistical study on dense molecular gas tracers of HCN (4–3), HCO^+ (4–3) lines and molecular tracers of [C I], and CO observations for a sample of 26 infrared bright star-forming (SF) galaxies. We investigate the dependence of dense gas star formation efficiency traced by HCN (4–3), HCO^+ (4–3) (that is $L_{IR}/L'_{HCN(4-3)}$, and $L_{IR}/L'_{HCO^+\ (4-3)}$), and luminosity ratio of $L'_{HCN(4-3)}/L'_{HCO^+\ (4-3)}$ on [C I]-CO ratios of $L'_{[CI](1-0)}/L'_{CO(1-0)}$, $L'_{[CI](2-1)}/L'_{CO(1-0)}$ and $L'_{[CI](2-1)}/L'_{[CI](1-0)}$ (hereafter $R_{[CI]}$) which are sensitive to interstellar medium conditions. Our findings show that both $L_{IR}/L'_{HCN(4-3)}$ and $L_{IR}/L'_{HCO^+\ (4-3)}$ have moderate correlations with $L'_{[CI](2-1)}/L'_{CO(1-0)}$ and $R_{[CI]}$, while $L'_{HCN(4-3)}/L'_{HCO^+\ (4-3)}$ does not show any significant correlations with any of the [C I]-CO ratios. We compare the $L'_{HCN(4-3)}/L'_{HCO^+\ (4-3)}$ ratios of AGN and SF galaxies, and find that although the higher $L'_{HCN(4-3)}/L'_{HCO^+\ (4-3)}$ ratios are mainly found in AGN, the majority of the $L'_{HCN(4-3)}/L'_{HCO^+\ (4-3)}$ values in SF galaxies are comparable to those in AGN. Based on our findings, it appears that the $L'_{HCN(4-3)}/L'_{HCO^+\ (4-3)}$ ratio may not be a reliable indicator of the presence of an AGN, although further investigation is needed to confirm this conclusion.

KEYWORDS

dense molecular gas, star formation-galaxies, sample, HCN (4–3), HCO + (4–3), AGN - active galactic nucleus

1 Introduction

In the past two decades, observational and theoretical studies have shown that molecular gas (Kennicutt, 1998; Bigiel et al., 2008; Daddi et al., 2010; Kennicutt and Evans, 2012), especially the dense molecular gas (Solomon et al., 1992; Gao and Solomon, 2004b; Gao and Solomon, 2004a; Wu et al., 2005; Gao et al., 2007; Baan et al., 2008; Chen et al., 2015; Bigiel et al., 2016; Zhang et al., 2014; Tan et al., 2018; Jiménez-Donaire et al., 2019; Jiang et al., 2020; Li et al., 2021) with a volume density of $n > 10^4\ cm^{-3}$ which can be traced by molecular emission lines with high critical densities as HCN and HCO^+, plays a significant role in star formation.

Using a large survey of HCN (1–0) emission from nearby normal spiral galaxies to ultraluminous infrared galaxies (ULIRGs), Gao and Solomon (2004b) found a tight linear correlation between the infrared (IR) and HCN luminosities. Observations on smaller scales, such as resolved galaxy structures (Chen et al., 2015; Chen et al., 2017; Usero et al., 2015; Bigiel et al., 2016; Shimajiri et al., 2017; Jiménez-Donaire et al., 2019), Galactic giant molecular clouds (GMCs) in the Milky Way (Wu et al., 2005; Wu et al., 2010; Lada et al., 2010; Lada et al., 2012; Evans et al., 2014), have shown that this linearity continues to large GMC associations and even individual dense cores in the Milky Way, spanning over eight orders of magnitude. Moreover, the $L'_{\rm HCN} - L_{\rm IR}$ correlation extends to possibly high-z galaxies and QSOs as well (Gao et al., 2007; Oteo et al., 2017).

In addition to HCN (1–0), linear correlations of $L'_{\rm dense} - L_{\rm IR}$ have also been found in many other dense gas tracers, e.g., HCO^+, HNC, CS, CN, CO and HCN with high-J transitions (Baan et al., 2008; Graciá-Carpio et al., 2008; Reiter et al., 2011; García-Burillo et al., 2012; Zhang et al., 2014; Liu et al., 2015; Oteo et al., 2017; Béthermin et al., 2018; Tan et al., 2018; Li et al., 2020; Li et al., 2021), in both Galactic dense cores and external galaxies. Baan et al. (2008) surveyed $\boldsymbol{J = 1–0}$ transitions of HCN, HNC, HCO^+, CN, as well as **CN (2–1)** and **CS (3–2)** in nearby LIRGs, and found strong relations between the integrated emissions of high-density tracer molecules with far-infrared luminosities. Liu et al. (2015) presented nine CO transitions (from $J = 4–3$ to $J = 12–11$) in a largest sample of 167 local galaxies, and found that all the nine CO transitions are linearly and tightly correlated with the far-infrared (far-IR) luminosities.

Using HCN (4–3), HCO^+ (4–3), and CS (7–6) observations in 20 nearby star-forming (SF) galaxies, Zhang et al. (2014) found tight and linear correlations between the luminosity of IR and that of molecular lines for all three dense gas tracers which probe molecular gas with density higher than 10^6 cm^{-3}. And this linear $L'_{\rm HCN(4-3)} - L_{\rm IR}$ correlation continues to Galactic dense clumps (Liu et al., 2016). Tan et al. (2018) mapped HCN (4–3) and HCO^+ (4–3) emissions in six nearby SF galaxies, which is part of the survey called Mapping the dense molecular gas in the strongest star-forming galaxies (MALATANG; PI: Y. Gao) with the JCMT telescope. They found that the measured linear $L'_{\rm dense} - L_{\rm IR}$ relations in nearby spatially resolved galaxies follow the linear correlations established globally in galaxies within the scatters, bridging the gap between Milky Way clouds and galaxy integrated observations. MALATANG is the first systematic survey of the spatially resolved observations of HCN (4–3) and HCO^+ (4–3) emissions with JCMT in a large sample of nearby galaxies. In the first stage of MALATANG, Tan et al. (2018) and Jiang et al. (2020) have observed 23 galaxies with six galaxies mapped in the central $2' \times 2'$ region (i.e., ~2 – 9 kpc) and the others mapped along the major axes. MALATANG-II expands the sample with 5 additional IR-bright galaxies in the EMPIRE (EMIR Multiline Probe of the ISM Regulating Galaxy Evolution) survey (Bigiel et al., 2016; Jiménez-Donaire et al., 2019). The details of the MALATANG description, sample, and data are given in Zhang et al. (in preparation, see also Tan et al., 2018; Jiang et al., 2020).

Recent observations, especially those involving large-scale mapping with high resolution, show that there is a linear relationship between $L'_{\rm dense}$ and $L_{\rm IR}$ from GMC in the Milky Way to high-z galaxies over ten orders of magnitude, whereas systematic variations are also observed among them. Based on the 62 HCN (1–0) observed positions across 29 nearby star-forming galaxies, Usero et al. (2015) found that the IR–to–HCN ratio (that is star formation efficiency of dense molecular gas, $\rm SFE_{dense}$) in nearby galaxy centers is ~6 – 8 times lower than that in the galaxy disks. With large-scale mapping of HCN (1–0) in M 51, Chen et al. (2015) and Bigiel et al. (2016) also found that the $\rm SFE_{dense}$ decreases in the nuclear region of M 51 when compared to the outer disk. Jiménez-Donaire et al. (2019) showed that the $\rm SFE_{dense}$ of EMPIRE galaxies as traced by HCN (1–0), HCO^+ (1–0), and HNC (1–0) increases with radius, and anti-correlates with stellar surface density, gas surface density, molecular-to-atomic gas ratio, and dynamical equilibrium pressure. However, the study of $\rm SFE_{dense}$ in NGC 253, using dense gas traced by HCN (4–3) and HCO^+ (4–3) emissions, show an increasing trend with respect to the stellar surface density (Jiang et al., 2020).

Comparing to the dense molecular gas tracers, CO and [C I] ($^3P_1 \rightarrow {}^3P_0$) [rest frequency: 492.161 GHz, hereafter [C I] (1–0)] and [C I] ($^3P_2 \rightarrow {}^3P_1$) [rest frequency: 809.344 GHz, hereafter [C I] (2–1)] lines are widely used as total molecular gas tracers in galaxies near and far (e.g., Weiß et al., 2003; Weiß et al., 2005; Papadopoulos et al., 2004; Papadopoulos and Greve, 2004; Bolatto et al., 2013; Dunne et al., 2022; Papadopoulos et al., 2022). Observations show that both [C I] emissions correlate well with CO emission in giant molecular cloud (Ikeda et al., 1999; Ikeda et al., 2002; Shimajiri et al., 2013), and even perform well in tracing molecular gas in local IR luminous objects (Israel et al., 2015; Krips et al., 2016; Jiao et al., 2017; Jiao et al., 2019), as well as star-forming galaxies at $z > 1$ (Popping et al., 2017; Valentino et al., 2018; Valentino et al., 2020; Boogaard et al., 2020), high-redshift sub-millimeter galaxies (SMGs, Alaghband-Zadeh et al. 2013; Yang et al. 2017) and protocluster galaxies (Lee et al., 2021). Theoretical models including turbulent (Offner et al., 2014; Glover et al., 2015), metallicity (Glover and Clark, 2016), and cosmic ray (Bisbas et al., 2015; Bisbas et al., 2017; Papadopoulos et al., 2018; Gaches et al., 2019) also predict widespread [C I] emission maps which are similar to CO maps.

Jiao et al. (2017) found that both [C I] luminosities of $L'_{\rm [CI](1-0)}$ and $L'_{\rm [CI](2-1)}$ are correlated linearly with $L'_{\rm CO(1-0)}$ for a sample of nearby (ultra)luminous infrared galaxies observed with the Herschel Space Observatory (*Herschel*), and the linear correlation between $L'_{\rm [CI](1-0)}$ with $L'_{\rm CO(1-0)}$ extends to SMGs up to z ≈ 6 (Dunne et al., 2022). Jiao et al. (2019) presented almost linear correlation between $L'_{\rm CO(1-0)}$ with both [C I] luminosities for a sample of nearby star-forming galaxies with a linear resolution around ~1kpc, while they also found that the $L'_{\rm [CI](2-1)}/L'_{\rm CO(1-0)}$ and $L'_{\rm [CI](2-1)}/L'_{\rm [CI](1-0)}$ (hereafter $R_{\rm [CI]}$) ratios varies within galaxies and shows centrally peaked in starbursts. Dunne et al. (2022) presented significant correlation between the $L'_{\rm [CI](1-0)}/L'_{\rm CO(1-0)}$ with both dust temperature and $L_{\rm IR}$. These results indicate that the [C I]-CO and $R_{\rm [CI]}$ ratios are expected to be sensitive to SFR intensity, due to CO dissociation by cosmic rays in high-SFR environments (Bisbas et al., 2015; Bisbas et al., 2017; Papadopoulos et al., 2018). Besides, the [C I]-CO ratios may be affected by AGN, as CO is significantly depleted by X-rays from the central AGN region (Meijerink and Spaans, 2005; Meijerink et al., 2007). Izumi et al. (2020) found that both $[CI](1–0)/^{12}CO(2–1)$ and $[CI](1–0)/^{13}CO(1–0)$ ratios tend to have higher values in AGNs compared to starburst and quiescent

galaxies. Moreover, the line ratio $R_{[CI]}$ can directly reflect excitation temperature in optically thin limit (Stutzki et al., 1997).

At present, the relationship between SFE_{dense} and local physical conditions, such as the stellar surface density and gas pressure is still under debate. [C I]-CO and $R_{[CI]}$ ratios are sensitive to the excitation temperature, star-formation and AGN activities. In this work, we have selected a sample that includes $J = 4–3$ emissions of HCN and/or HCO+, as well as [C I] and CO (1–0) observations. Our aim is to investigate the possible correlation between the SFE_{dense} with dense gas traced by HCN (4–3) and/or HCO^+ (4–3) and the [C I]-CO ratios. We also aim to investigate the reliability of using $L'_{HCN\,(4-3)}/L'_{HCO^+\,(4-3)}$ ratio as an indicator of AGN. This paper is structured as follows. In Section 2, we describe our sample selection and data reduction method. The results and discussion are presented in Section 3. In the last section we summarize the main conclusions.

2 Sample and data reduction method

Systematic survey of HCN (4–3), HCO^+ (4–3), and both [C I] emissions are rare. The sample discussed here consists of sources with available observations of HCN (4–3) and/or HCO^+ (4–3), and [C I] (1–0) and/or [C I] (2–1), which are currently as comprehensive as possible based on literature. We finally obtained three subsamples named: Tan18, Zhang14, and Imanishi18, respectively. The subsample of Tan18 consists of five spatially resolved nearby star-forming galaxies that were selected by cross-matching the MALATANG sample in Tan et al. (2018) and [C I] mapping from Jiao et al. (2019). Zhang et al. (2014) reported HCN (4–3) and HCO^+ (4–3) observations in 20 nearby star-forming galaxies with the Atacama Pathfinder EXperiment (APEX) 12 m telescope. By cross matching the galaxies in Zhang et al. (2014) with [C I] data observed with *Herschel* in Lu et al. (2017) and Fernández-Ontiveros et al. (2016), we finally obtain fifteen galaxies defined as subsample of Zhang14. We check the galaxies in Imanishi et al. (2018), and find five of them have [C I] observations in literature (e.g., Fernández-Ontiveros et al., 2016; Kamenetzky et al., 2016; Jiao et al., 2017). We further add galaxy NGC 7469 which has ALMA observations of HCN (4–3), HCO^+ (4–3), and [C I] from Izumi et al. (2015), Izumi et al. (2020), and define these six galaxies as subsample of Imanishi18. The Tan18 and Zhang14 samples consist of IR bright galaxies with $S_\nu(100\,\mu m) > 100 Jy$, which was selected from Infrared Astronomical Satellite (IRAS) Revised Bright Galaxy Sample (Sanders et al., 2003). Meanwhile, the Imanishi18 galaxies are classified as ULIRGs with $L_{IR} > 10^{12}\,L_\odot$, except for IRAS 04315-0840 which is categorized as a LIRG with $L_{IR} \sim 5\times10^{11}\,L_\odot$. In brief, the three subsamples encompasses galaxies with L_{IR} ranging from $10^{10}\,L_\odot$ to $10^{12.5}\,L_\odot$, including nearby normal star-forming galaxies, starbursts, and AGN galaxies. The basic information of each galaxy in our sample is shown in Table 1.

2.1 Data reduction for Tan18 subsample

The HCN (4–3) and HCO^+ (4–3) data in subsample Tan18 are from Tan et al. (2018) which were observed by JCMT with FWHM ~14″ at 350 GHz with grid spacing of 10″, and the [C I] data is obtained from Jiao et al. (2019) which was observed by *Herschel* with FWHM ~38.6″ and ~36.2″ at 492 GHz (the rest frequency of [C I] (1–0)) and 809 GHz (the rest frequency of [C I] (2–1), Makiwa et al., 2013), respectively. In Supplementary Figure S1, we present the distribution of [C I] (1–0) integrated intensities with detections (signal-to-noise ratio of SNR >3σ) of HCN (4–3) and HCO^+ (4–3) shown as red and blue dashed squares. We further use the luminosity ratios of $L'_{[CI]\,(1-0)}/L'_{CO\,(1-0)}$, $L'_{[CI]\,(2-1)}/L'_{CO\,(1-0)}$, and $R_{[CI]}$ results from Jiao et al. (2019) with CO (1–0) (Kuno et al., 2007; Salak et al., 2013) observed using Nobeyama 45-m telescope. The fluxes of [C I] lines in Jiao et al. (2019) were determined by fitting the observed line profiles with the instrumental Sinc function after subtracting a fifth-order polynomial fit of the continuum emission (see details in Lu et al. 2017; Jiao et al. 2019). Then flux was converted to luminosity following Papadopoulos et al. (2012). The CO (1–0) images were smoothed to match both [C I] maps using convolution kernels generated by comparing the Nobeyama 45-m profile with the *Herschel* Gaussian profile of FWHM ~38.6″ and ~36.2″ (Aniano et al., 2011), respectively. Jiao et al. (2019) calculated the $R_{[CI]}$ directly for each pixel without beam matching since the FWHMs of [C I] (1–0) and [C I] (2–1) are similar.Column (1) and (2): the sub-samples and galaxy names. Tan18 refers to Tan et al. (2018), Zhang14 refers to Zhang et al. (2014), and Imanishi18 refers to Imanishi et al. (2018). Columns (3)–(5) are the coordinate and velocity adopted from NASA/IPAC Extragalactic Database (NED). Columns (6) and (7): the FWHM of the beam size for HCN (4–3) observations in arcseconds and physical scale of kiloparsec, respectively. 3 × 3 in parentheses of column (6) represents the Gaussian fits region of the spatially extended galaxy IRAS 04315-0840. The values in column (7) with "~" means geometric mean physical scales for synthesized beams of ALMA observations. Column (8): galaxy types. The type of "Cp" in sub-sample of Imanishi18 refers to starburst + AGN composities.

The luminosities of $L'_{HCN\,(4-3)}$ and $L'_{HCO+\,(4-3)}$ are adopted from Tan et al. (2018). Briefly, the luminosities of HCN (4–3) and HCN (4–3) were estimated by subtracting a first-order baseline and then integrating the velocity range which was determined based on CO(1–0) data using a Gaussian fitting. We also take the total infrared (3–1,100 μm) luminosities L_{IR} from Tan et al. (2018) which were estimated with the prescription of Galametz et al. (2013): $L_{IR} = \Sigma c_i \nu L_\nu(i) L_\odot$ using calibrated IR image data including *Spitzer* MIPS 24 μm and *Herschel* 70 μm, 100 μm and 160 μm from the NASA/IPAC Infrared Science Archive (IRSA), where c_i is the calibration coefficient as shown in Table 3 of Galametz et al. (2013), and $\nu L_\nu(i)$ is the luminosity in a given band i in unit of $L_\odot$. The FWHM of the MIPS 24 μm is 6″[1], and the Herschel instrument provides maps with FWHMs of ~ 5.6″, 6.8″, and 10.7″ at 70 μm, 100 μm, and 160 μm[2], respectively. The IR images are smoothed to match the JCMT line observations with convolution kernels generated by comparing the *Spitzer* and *Herschel* profiles with Gaussian profile of FWHM 14″(Aniano et al., 2011). Same as Tan et al. (2018), the total uncertainties of L_{IR} comprise the flux uncertainty (~5%) and the uncertainty from combined luminosities

1 https://irsa.ipac.caltech.edu/data/SPITZER/docs/mips/mipsinstrumentha ndbook/

2 https://www.cosmos.esa.int/web/herschel/pacs-overview

TABLE 1 The basic properties of the galaxies for the three subsamples.

Sample	Name	R.A. (hh:mm:ss)	Decl (dd:mm:ss)	V_h (km s^{-1})	HCN FWHM ($''$)	HCN physical scale (kpc)	Type
(1)	(2)	(3)	(4)	(5)	(6)	(7)	(8)
Tan18	M 82	09:55:52.7	+69:40:45.8	203	14	0.24	SF
	M 83	13:37:00.9	−29:51:55.5	513	14	0.33	SF
	NGC 253	00:47:33.1	−25:17:17.6	243	14	0.24	SF
	NGC 1068	02:42:40.7	−00:00:47.8	1,137	14	1.1	AGN
	NGC 6946	20:34:52.3	+60:09:14.1	40	14	0.32	SF
Zhang14	IC 1623	01:07:47.2	−17:30:25.3	6,016	18	7.2	SF
	NGC 3256	10:27:51.3	−43:54:13.5	2,804	18	3.9	SF
	NGC 4418	12:26:54.6	−00:52:39.4	2,179	18	2.6	AGN
	IRAS 13120−5453	13:15:06.4	−55:09:23.2	9,222	18	11.2	AGN
	NGC 6240	16:52:58.9	+02:24:03.3	7,339	18	9.3	AGN
	IRAS 17578−0400	18:00:31.9	−04:00:53.3	4,210	18	5.3	SF
	IRAS 18293−3413	18:32:41.1	−34:11:27.2	5,449	18	6.8	SF
	NGC 7469	23:03:15.6	+08:52:26.4	4,892	18	6.2	AGN
	NGC 7552	23:16:10.8	−42:35:05.1	1,608	18	1.7	SF
	NGC 7771	23:51:24.8	+20:06:42.3	4,277	18	5.5	SF
	Mrk 331	23:51:26.8	+20:35:09.9	5,541	18	7.1	AGN
	Arp 220	15:34:57.3	+23:30:11.3	5,434	14	5.4	AGN
	Mrk 231	12:56:14.2	+56:52:25.2	12,642	14	12.3	AGN
	NGC 4945	13:05:27.5	−49:28:05.6	1,96	18	0.33	AGN
	IC 342	03:46:48.5	+68:05:46.9	31	20	0.38	SF
Imanishi18	IRAS 08572 + 3915	09:00:25.4	+39:03:54.4	17,493	1.8 × 1.1	~1.5	AGN
	IRAS 19254−7245 (Superantennae)	19:31:21.4	−72:39:18.0	18,500	0.76 × 0.44	~0.69	AGN
	IRAS 22491−1808	22:51:49.3	−17:52:23.5	23,312	0.6 × 0.6	0.90	AGN
	IRAS 04315−0840 (NGC 1614)	04:33:59.9	−08:34:44.0	4,778	1.5 × 1.3 (3 × 3)	0.96	Cp
	IRAS 13451 + 1232	13:47:33.4	+12:17:24.2	36,497	0.69 × 0.58	~1.42	AGN
	NGC 7469_A + B + C + D	23:03:15.6	+08:52:26.4	4,892	0.5 × 0.4	~0.15	AGN

(~20% for galaxies with more than four IR bands available and ~25% for less than four IR bands, Galametz et al., 2013).

In MALATANG-I observations, M 83 was detected in HCN (4–3) and HCO$^+$ (4–3) emissions at only the central position (Tan et al., 2018). However, more detections are found for M 83 by combining the MALATANG-I and MALATANG-II data. In this work, we use the combined data for M 83. The HCN (4–3) and HCO$^+$ (4–3) detections of M 83 are also shown in Supplementary Figure S1.

2.2 Data reduction for Zhang14 subsample

The HCN (4–3) and HCO$^+$ (4–3) emissions in the subsample of Zhang14 from Zhang et al. (2014) are mostly observed by the APEX in the central region with FWHM ~18$''$, and collected from literature with FWHM ~14$''$ – 18$''$. While the IR luminosity of the entire galaxy $L_{\rm TIR}$ is adopted from Sanders et al. (2003). In order to estimate the $L_{\rm TIR}$ within the same beam size as HCN (4–3) and HCO$^+$ (4–3), Zhang et al. (2014) used *Herschel* PACS 100 μm or 70 μm (when 100 μm is not available) images to perform aperture photometry both with the submillimeter beam size and the whole galaxy. The beam size correction IR luminosity is estimated as $L_{\rm IR} = L_{\rm TIR} \times R_{\rm SD} \times C_{\rm aper}$ (see the details in Zhang et al., 2014), where $R_{\rm SD}$ is the ratio of flux densities within the beam size of the HCN (4–3) and HCO$^+$ (4–3) emissions to that measured in the whole galaxy, and $C_{\rm aper}$ is the aperture correction factor for the beam size. The total uncertainty estimated for $L_{\rm IR}$ is 20{%}. We note that the majority of galaxies have a $R_{\rm SD} = 1$, which means that their

TABLE 2 The galaxy in Zhang14.

Galaxy	Dis (Mpc)	$L_{IR}(10^{10}L_{\odot})$	L'_{HCN}	L'_{HCO^+}	R_{SD}	C_{aper}	$I_{[CI](1-0)}$	$I_{[CI](2-1)}$	$I_{CO(1-0)}$
			(10^6Kkms^{-1}pc^2)				(Jykms^{-1})		
(1)	(2)	(3)	(4)	(5)	(6)	(7)	(8)	(9)	(10)
IC 1,623	82.4	49.0	<62	62 ± 15	0.65	1.29	1,227.0 ± 88.8	1,160.6 ± 18.5	557.0 ± 111.9
NGC 3,256	44.3	57.5	22 ± 4	56 ± 4	0.34	1.29	4,064.5 ± 177.3	4,996.6 ± 43.8	1,222.8 ± 366.9
NGC 4,418	29.5	9.33	26.8 ± 2.0	8.9 ± 1.8	1.0	1.0	<752.0	470.0 ± 50.7	137.9 ± 24.5
IRAS 13120–5,453	128.3	178	330 ± 30	265 ± 30	1.0	1.0	1,349.6 ± 149.0	1,537.9 ± 32.3	…
NGC 6240	107	70.8	189 ± 30	260 ± 20	1.0	1.0	1,598.3 ± 106.2	3,515.1 ± 104.5	290.9 ± 44.3
IRAS 17578–0400	61.1	24.5	57.0 ± 10	<34	1.0	1.0	<1,266.1	676.1 ± 55.8	…
IRAS 18293–3413	77.4	64.6	<55	116 ± 20	1.0	1.0	2,591.8 ± 138.3	2,378.2 ± 28.4	686.1 ± 205.8
NGC 7469	71.6	46.8	<30	37 ± 10	1.0	1.0	1,219.7 ± 79.2	1,464.1 ± 17.6	298.0 ± 89.4
NGC 7552	19.5	8.91	5.1 ± 0.4	9.4 ± 0.4	0.59	1.29	3,178.2 ± 176.4	3,943.9 ± 40.8	652.0 ± 195.6
NGC 7771	63.0	26.9	<36	<36	0.55	1.29	1,509.3 ± 105.5	1,247.3 ± 21.6	370.3 ± 84.2
Mrk 331	80.9	33.9	60 ± 13	<40	1.0	1.0	860.1 ± 64.4	877.7 ± 14.9	371.2 ± 86.2
Arp 220	79.9	162.2	950 ± 190	170 ± 40	1.0	1.0	1,820.8 ± 297.2	1,737.7 ± 64.2	445.3 ± 85.3
Mrk 231	180.8	340	550 ± 110	188 ± 23	1.0	1.0	<404.7	446.7 ± 17.8	103.6 ± 37.4
NGC 4945	3.8	2.82	3.6 ± 0.05	4.5 ± 0.05	0.40	1.29	13,237.9	34,333.9	…
IC 342	3.9	1.08	0.8 ± 0.2	…	0.05	1.33	5,566.1 ± 554.1	8,124.8 ± 299.5	…

corresponding beam size of HCN (4–3) and HCO^+ (4–3) can cover the entire galaxy.

The majority of [C I] lines used in this study are taken from Lu et al. (2017), and the corresponding galaxy is point-like with respect to the *Herschel* beam at [C I] (2–1) rest frequency, except for NGC 4945 and IC 342 which are obtained from Fernández-Ontiveros et al. (2016). The CO (1–0) are adopted from Jiao et al. (2017) with beam size greater than that of [C I] (2–1). Specifically, the [C I] (1–0) of Galaxy NGC 4418 was flagged as quality Q = 4 ($3 \leq$ SNR <5) in Lu et al. (2017), which means that the [C I] (1–0) is only a possible line identification with the inferred line velocity being just short of satisfying their velocity criterion. Considering the low SNR of NGC 4418, we define the galaxy as non-detection with 3σ as upper limit. Table 2 lists the targets of subsample Zhang14 with distance, intensities, luminosities, and correction factors of R_{SD}, C_{aper}. We adopt 3σ upper limits for non-detections.

2.3 Data reduction for Imanishi18 subsample

The HCN (4–3) and HCO^+ (4–3) emissions of subsample Imanishi18 are taken from Table 15 in Imanishi et al. (2018) that were observed with ALMA, and the corresponding L_{IR} values are also adopted from Imanishi et al. (2018). In this sample of galaxies, the ALMA measurements mostly cover the emissions of HCN (4–3) and HCO^+ (4–3). This is because ULIRGs are typically dominated by nuclear compact energy sources with $\lesssim$500 pc (Soifer et al., 2000), and the dense gas tracers mostly come from compact nuclear regions. The luminosities of HCN (4–3) and HCO^+ (4–3) were measured using Gaussian fits of the spectra within the beam size. However, for the spatially extended galaxy IRAS 04315–1808, the luminosity was estimated from Gaussian fits ($3'' \times 3''$) of the spatially integrated spectra. The CO (1–0) and [C I] intensities are collected from literature as shown in Table 3.

Particularly, with unprecedented high resolution ALMA observation, NGC 7469 is regarded as an AGN position of A, and three bright knots in the starburst ring as B, C, and D (see the details in Izumi et al., 2015). In Table 4, we present the $L'_{HCN\,(4-3)}/L'_{HCO^+\,(4-3)}$ ratio (adopted from Table 3 from Izumi et al., 2015) that both emissions were extracted within a single synthesized beam with 150 pc resolution for the four positions. The CO (1–0) and [C I] (1–0) luminosities are adopted from Table 7 from Izumi et al. (2020) within ~130 pc aperture. In the following analysis, we directly use $L'_{HCN\,(4-3)}/L'_{HCO^+\,(4-3)}$, [C I] (1–0), and CO (1–0) values of NGC 7469 without correction since their beam sizes are similar to each other.

The three subsample datasets are obtained from diverse telescope observations with distinct beam sizes, particularly for HCN (4–3) and HCO^+ (4–3) observations. In Table 1, we list the FWHM of HCN (4–3) for each galaxy (the FWHMs of HCN (4–3) and HCO^+ (4–3) are similar). The [C I] observations for all galaxies were obtained with *Herschel*, except for NGC 7469 which was observed with ALMA. Notablely, the line ratios of IR-HCN/HCO^+ and $L'_{HCN\,(4-3)}/L'_{HCO^+\,(4-3)}$, as well as

TABLE 3 ALMA sample in Imanishi.

Galaxy	Redshift	log $L_{IR}(L_\odot)$	L'_{HCN}	L'_{HCO^+}	$I_{CO(1-0)}$ (Jykms^{-1})	Ref_CO	$I_{[CI](1-0)}$	$I_{[CI](2-1)}$	Ref_CI
			(10^7Kkms^{-1}pc^2)				(Jykms^{-1})		
(1)	(2)	(3)	(4)	(5)	(6)	(7)	(8)	(9)	(10)
IRAS 08572 + 3915	0.0580	12.1	5.1 ± 0.5	6.6 ± 0.5	9.0 ± 3.2	So97	<1,140	<179	Ka16
IRAS 19254–7245	0.0617	12.1	18 ± 1	11 ± 1	64.8 ± 13.0[a]	Mi90	…	292 ± 54	Ka16
IRAS 22491–1808	0.0776	12.2	21 ± 1	15 ± 1	31.5 ± 6.3[b]	Sa91	…	<177	Ka16
IRAS 04315–0840	0.0160	11.7	0.34 ± 0.10	1.9 ± 0.2	247.7 ± 37.8	Ji17	<799.1	897.8 ± 24.1	Lu17
IRAS 13451 + 1232	0.1215	12.3	12 ± 2	22 ± 2	20 ± 6	DC11	…	172.2	Fa16

TABLE 4 NGC 7469.

Galaxy	$L'_{HCN(4-3)}/L'_{HCO^+(4-3)}$	$L'_{CO(1-0)}$	$L'_{[CI](1-0)}$
		(10^6Kkms^{-1}pc^2)	
NGC 7469_A	1.11 ± 0.06	23.2 ± 1.1	21.4 ± 0.4
NGC 7469_B	0.75 ± 0.11	19.0 ± 0.3	4.7 ± 0.1
NGC 7469_C	0.45 ± 0.07	15.3 ± 0.3	3.5 ± 0.1
NGC 7469_D	0.48 ± 0.04	20.9 ± 0.3	5.0 ± 0.1

[C I]-CO ratios are calculated at the same resolutions for the Tan18 sample. For the Zhang14 and Imanishi18 samples, most galaxies are point sources with respect to the corresponding FWHM. Therefore, the observed HCN (4–3), HCO^+ (4–3), [C I], and CO emissions represent the average properties of the galaxies. Furthermore, aperture corrections are applied for a few extended sources in Zhang14, and spatial Gaussian fits are used for spatially resolved galaxy of IRAS 04315–1808 in the Imanishi18 sample. Meanwhile, NGC 7469 use similar resolutions of HCN (4–3), HCN (4–3), [C I] and CO data. We also test the influence of beam size on line ratios for spatially resolved sample Tan18 and NGC 7469, and find that the correlations of beam size in kpc scale with $L_{IR}/L'_{HCN(4-3)}$ and $L_{IR}/L'_{HCO^+(4-3)}$ are −0.17 and 0.14 (these two line ratios and $L'_{HCN(4-3)}/L'_{HCO^+(4-3)}$ are what we mainly discuss in next section), respectively. The correlation between beam size and $L'_{HCN(4-3)}/L'_{HCO^+(4-3)}$ is 0.39, which becomes 0.29 after removing the center point of NGC 1068. This center point could be associated with the significantly high $L'_{HCN(4-3)}/L'_{HCO^+(4-3)}$ ratios that are correlated with the UV/X-ray illumination by AGN (García-Burillo et al., 2014; Viti et al., 2014; Tan et al., 2018). Consequently, the impact of varying beam sizes on the overall sample is minimal.

Columns 2 to 7 are adopted from Zhang et al. (2014). R_{SD} is the ratio of flux densities within the beam size of HCN (4–3) to that measured in the whole galaxy, and C_{aper} is the aperture correction factor for the beam size (see the details in Zhang et al., 2014). [C I] fluxes in columns 8 and 9 are adopted from Lu et al. (2017), except for NGC 4945 and IC 342 which obtained from Fernández-Ontiveros et al. (2016). Column 10 is the CO (1–0) fluxes adopted from Jiao et al. (2017). Columns 2 and 3 are the redshift and infrared luminosities adopted from Imanishi et al. (2018), column 4 and 5 are the HCN (4–3) and HCO^+ (4–3) luminosities which are adopted from Table 15 in Imanishi et al. (2018). Columns 6 and 7 are CO (1–0) intensities and references: So97—Solomon et al. (1997), Mi90—Mirabel et al. (1990), Sa91—Sanders et al. (1991), Ji17—Jiao et al. (2017), DC11—Dasyra and Combes (2011). Columns 8, 9, and 10 are [C I] intensities and references: Ka16—Kamenetzky et al. (2016), Lu17—Lu et al. (2017), Fa16—Fernández-Ontiveros et al. (2016). [a] The CO (1–0) data is observed with SEST, and is converted from K km s^{-1} to Jy km s^{-1} with conversion factor S_ν/T (Jy/K) = 27.[b] The CO (1–0) data is observed with 12m NRAO, and is converted from K km s^{-1} to Jy km s^{-1} with conversion factor S_ν/T (Jy/K) = 35.The A, B, C, and D of NGC 7469 stand for the AGN position and three bright knots in the starburst ring (see details in Izumi et al., 2015). The $L'_{HCN(4-3)}/L'_{HCO^+(4-3)}$ is adopted from Izumi et al. (2015), and CO (1–0) and [C I] (1–0) luminosities are adopted from Izumi et al. (2020).

2.4 WISE data

We also use the Wide-field Infrared Survey Explorer (WISE) 3.4 μm (W1) and 4.6 μm (W2) emissions and uncertainties for each galaxy from the NASA/IPAC Infrared Science Archive. For the samples of Tan18 and Zhang14, we firstly estimate the background for each galaxy using SExtractor (Source-Extractor; Bertin and Arnouts, 1996) program with the corresponding uncertainty maps as inputs, and then subtract its estimated background. The background-subtracted image of each galaxy is smoothed to its corresponding HCN (4–3) resolution (JCMT or APEX) with convolution kernels generated by comparing the WISE profiles with JCMT/APEX Gaussian profile of FWHM 14″/18″(Aniano et al., 2011). For galaxies in sample of Imanish18 with high resolutions (observed with ALMA with FWHM mostly smaller than 1″at HCN (4–3) and HCO^+ (4–3)), we directly use its profile-fit photometry magnitude from "WISE All-Sky Source Catalog" at IPAC.

The WISE images are originally in units of digital numbers (DN), and we convert them to luminosity units of $L_\odot$ with method shown in Supplementary Material. Similar to Tan et al. (2018), in order to convert the units from $L_\odot$ into $L_\odot$ beam^{-1}, we scale the image by a factor of $1.133 \times (FWHM/pixel\ size)^2$, where FWHM = 14″for JCMT and 18″for APEX, pixel size is the length of a pixel in arcseconds. As shown in Supplementary Material, the WISE uncertainties include the zero-point magnitude uncertainty, and the instrumental uncertainty measured with WISE uncertainty maps.

3 Results and discussion

3.1 Correlations between SFE_{dense} with [C I]-CO luminosity ratios

The MALATANG HCN (4–3) and HCO^+ (4–3) mappings do not satisfy Nyquist sampling theorem with grid spacing of 10″ for the JCMT FWHM of ~14″ at 350 GHz, so we directly use the luminosity ratios of $L_{IR}/L'_{HCN\,(4-3)}$ and $L_{IR}/L'_{HCO^+\,(4-3)}$ under JCMT scale from Tan et al. (2018), and compare them with [C I]-CO ratios under *Herschel* scales. As shown in Supplementary Figure S1, for pixels which have more than one JCMT detection points, we use their mean values of $L_{IR}/L'_{HCN\,(4-3)}$, $L_{IR}/L'_{HCO^+\,(4-3)}$ or $L'_{HCN\,(4-3)}/L'_{HCO^+\,(4-3)}$ as its final values, respectively.

Figure 1 shows the correlations between $L_{IR}/L'_{HCN\,(4-3)}$ with $L'_{[C\ I]\ (1-0)}/L'_{CO\ (1-0)}$, $L'_{[C\ I]\ (2-1)}/L'_{CO\ (1-0)}$, and $R_{[CI]}$ for three subsamples combined. The scatter plots show that $L_{IR}/L'_{HCN\,(4-3)}$ almost has no correlation with $L'_{[C\ I]\ (1-0)}/L'_{CO\ (1-0)}$, while correlates moderately with both $L'_{[C\ I]\ (2-1)}/L'_{CO\ (1-0)}$ and $R_{[CI]}$. Besides, for *Herschel* pixel points where multiple MALATANG sample detections were made, we also use the original values of $L_{IR}/L'_{HCN\,(4-3)}$, and present the correlations of $L_{IR}/L'_{HCN\,(4-3)}$ with [C I]-CO luminosity ratios in panel A of Supplementary Figure S2 for all subsamples combined in Supplementary Material. Supplementary Figure S2, 1 show that using the original values of the MALATANG sample produces similar results to the mean values of the sample.

We further use Monte Carlo method to estimate the Spearman's rank correlation with those limits. For the upper limits (as U_{upper}), we generate 10,000 uniformly distributed random numbers ranging from 0 to U_{upper}. And for the lower limits (as U_{lower}), the 10,000 random numbers are uniformly distributed over U_{lower} to $10^3 U_{lower}$. We then calculate the correlation coefficient 10,000 times using the detection points and the generated random numbers for the limits, and define the average r and p as the final results. As shown in Table 5, the results obtained with and without limits are similar. Moreover, $L_{IR}/L'_{HCN\,(4-3)}$ moderately correlates with $L'_{[C\ I]\ (2-1)}/L'_{CO\ (1-0)}$ and $R_{[CI]}$, while it has no significant correlation with $L'_{[C\ I]\ (1-0)}/L'_{CO\ (1-0)}$.

We further plot the $L_{IR}/L'_{HCO^+\,(4-3)}$ against $L'_{[C\ I]\ (1-0)}/L'_{CO\ (1-0)}$, $L'_{[C\ I]\ (2-1)}/L'_{CO\ (1-0)}$, and $R_{[CI]}$ for three subsamples together using mean values of MALATANG points in Figure 2, and list the Spearman's rank correlation coefficients in Table 5. The correlation coefficients with both lower and upper limits are also listed in Table 5. We also present the $L_{IR}/L'_{HCO^+\,(4-3)}$ results of the total sample with original values of MALATANG detections in panel B of Supplementary Figure S2, respectively. The $L_{IR}/L'_{HCO^+\,(4-3)}$ has moderate correlation with all three line luminosity ratios when analyzing the mean values of MALATANG points. However, when considering the total sample with original values, the correlations between $L_{IR}/L'_{HCO^+\,(4-3)}$ and both $L'_{[C\ I]\ (2-1)}/L'_{CO\ (1-0)}$ and $R_{[CI]}$ are slightly stronger than the correlation between $L_{IR}/L'_{HCO^+\,(4-3)}$ and $L'_{[C\ I]\ (1-0)}/L'_{CO\ (1-0)}$, as shown in Supplementary Figure S2. Columns (2)–(7): The Spearman's rank correlation coefficient (r) and the possibility of no correlation (p) without (first row) and with (second row) non-detection points.

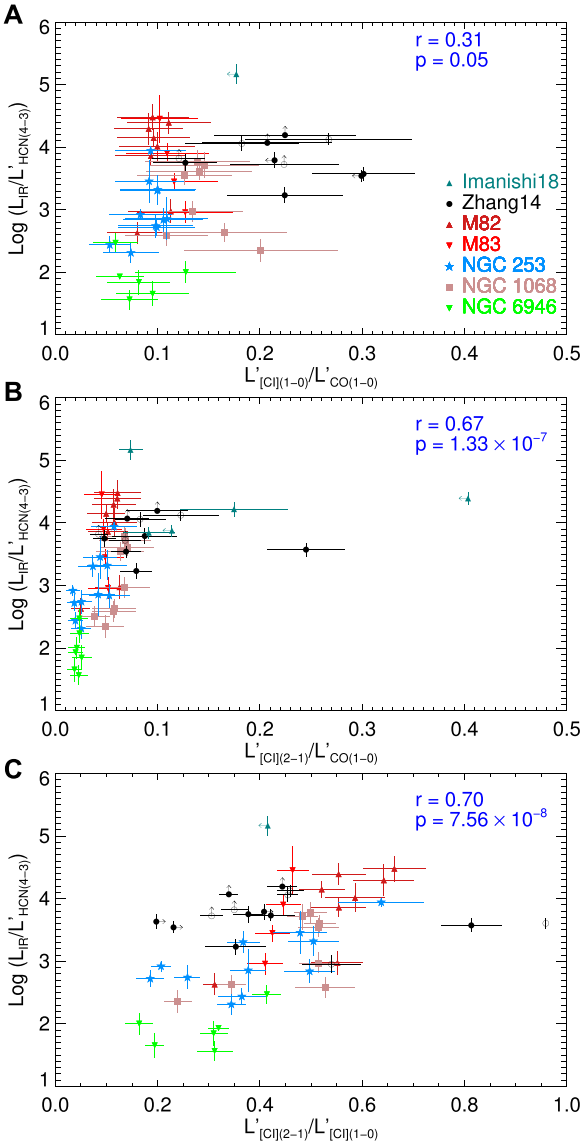

FIGURE 1
Comparison of the luminosity ratios of $L_{IR}/L'_{HCN\,(4-3)}$ with the line luminosity ratios of $L'_{[CI]\ (1-0)}/L'_{CO\,(1-0)}$ **(A)**, $L'_{[CI]\ (2-1)}/L'_{CO\,(1-0)}$ **(B)**, and $L'_{[CI]\ (2-1)}/L'_{[CI]\ (1-0)}$ **(C)**, respectively. The labeled r and p represent the Spearman's rank correlation coefficient and the possibility of no correlation for the detection points. Our literature samples include five resolved nearby galaxies (M 82, M 83, NGC 253, NGC 1068, and NGC 6946 shown as colored symbols) adopted from Tan et al. (2018), and fifteen star-forming galaxies from Zhang et al. (2014) shown as black circles, and five ((U)LIRGs) that contain AGNs adopted from Imanishi et al. (2018) shown as teal triangles. The filled and hallow black circles represent galaxies from Zhang et al. (2014) that do not need and need IR luminosity corrections, respectively. The arrows denote 3σ limits.

3.2 The $L'_{HCN\,(4-3)}/L'_{HCO+\,(4-3)}$

In Figure 3, we present the correlation between $L'_{HCN\,(4-3)}/L'_{HCO^+\,(4-3)}$ and $L'_{[C\ I]\ (1-0)}/L'_{CO\ (1-0)}$, $L'_{[C\ I]\ (2-1)}/L'_{CO\ (1-0)}$, and $R_{[CI]}$ for three subsamples. These correlations are calculated

TABLE 5 The Spearman's rank correlation coefficients and significance.

Parameters	$L'_{[CI]\ (1-0)}/L'_{CO\,(1-0)}$		$L'_{[CI]\ (2-1)}/L'_{CO\,(1-0)}$		$L'_{[CI]\ (2-1)}/L'_{[CI]\ (1-0)}$	
	r	p	r	p	r	p
(1)	(2)	(3)	(4)	(5)	(6)	(7)
$L_{IR}/L'_{HCN\,(4-3)}$	0.31	0.05	0.67	1.33×10^{-7}	0.70	7.56×10^{-8}
	0.39	7.46×10^{-3}	0.65	4.09×10^{-7}	0.51	1.11×10^{-4}
$L_{IR}/L'_{HCO+\,(4-3)}$	0.53	2.81×10^{-4}	0.78	3.46×10^{-11}	0.54	1.24×10^{-4}
	0.50	1.26×10^{-3}	0.72	5.92×10^{-8}	0.51	1.16×10^{-4}
$L'_{HCN\,(4-3)}/L'_{HCO+\,(4-3)}$	0.34	0.09	0.25	0.22	−0.29	0.18
	0.20	0.31	0.09	0.64	0.03	0.80

using the mean values of the MALATANG subsample for points which have more than one JCMT detections in *Herschel* pixel. The four regions of NGC 7469 resolved with ALMA (AGN position A, and three bright starburst knots B, C, D) are also included. Table 5 gives the Spearman's rank correlation coefficients for samples together without and with considering the limits. We also present these correlations for total samples using the original values of MALATANG detections in Supplementary Figure S2. There is no obvious correlation between $L'_{HCN\,(4-3)}/L'_{HCO^+\,(4-3)}$ and $L'_{[C\ I]\ (1-0)}/L'_{CO\ (1-0)}$, $L'_{[C\ I]\ (2-1)}/L'_{CO\ (1-0)}$, or $R_{[CI]}$, while the $L'_{HCN\,(4-3)}/L'_{HCO^+\,(4-3)}$ in some galaxies (e.g., NGC 1068, few galaxies in Zhang14) shows slightly higher than the other galaxies.

The L'_{HCN}/L'_{HCO+} ratio has been proposed as an indicator of AGN activity due to higher L'_{HCN}/L'_{HCO+} observed in galaxies hosting AGN (e.g., Krips et al., 2008; Izumi et al., 2013; Izumi et al., 2015; Izumi et al., 2016; Privon et al., 2015; Imanishi et al., 2018). In panel A of Figure 4, we present a box plot to show the mean ratio, interquartile range, and full range of the $L'_{HCN\,(4-3)}/L'_{HCO^+\,(4-3)}$ of the Tan18 sample and total sample separated into galaxy types of star-forming galaxies and AGN. For Seyfert 2 galaxy of NGC 1068, the $L'_{HCN\,(4-3)}/L'_{HCO^+\,(4-3)}$ in the central AGN region is obvious higher than other regions. While for SF galaxies in Tan18, the $L'_{HCN\,(4-3)}/L'_{HCO^+\,(4-3)}$ ratio in the center are comparable with those in other regions. In the entire sample, the distributions of $L'_{HCN\,(4-3)}/L'_{HCO^+\,(4-3)}$ for AGN is generally higher than that for SF galaxies, but there are also large overlap regions.

Using the WISE surveys in COSMOS field, Stern et al. (2012) present a simple mid-infrared color criterion of W1 − W2 ≥ 0.8 for W2 < 15.05 mag which identifies a reliable and complete AGN sample. In order to test the $L'_{HCN\,(4-3)}/L'_{HCO^+\,(4-3)}$ with AGNs, we present the $L'_{HCN\,(4-3)}/L'_{HCO^+\,(4-3)}$ ratios with AGN diagnostic of W1 − W2 colors in panel B of Figure 4. All of the W2 in our sample is smaller than the criterion of 15.05 mag. The high $L'_{HCN\,(4-3)}/L'_{HCO^+\,(4-3)}$ ratios are mostly found in the region where W1 − W2 is greater than 0.8 mag. However, in this region, the $L'_{HCN\,(4-3)}/L'_{HCO^+\,(4-3)}$ ratios vary widely, ranging from a minimum of 0.5, which is similar to the values in the region where W1 − W2 is less than 0.8 mag for star-forming points, to a maximum of 5.5, which is significantly higher than most star-forming regions. Meanwhile, most of the $L'_{HCN\,(4-3)}/L'_{HCO^+\,(4-3)}$ values in the region of W1 − W2 < 0.8 mag are comparable with those values in the region of W1 − W2 ≥ 0.8 mag. This is consistent with panel A of Figure 4, and both indicate that AGN may enhance the ratio of $L'_{HCN\,(4-3)}/L'_{HCO^+\,(4-3)}$ in some systems, while most values of $L'_{HCN\,(4-3)}/L'_{HCO^+\,(4-3)}$ are similar to those in SF systems. Therefore, the reliability of using the $L'_{HCN\,(4-3)}/L'_{HCO^+\,(4-3)}$ ratio as an AGN indicator may be compromised, as discussed in the following.

3.3 Discussion

3.3.1 The relationship between SFE_{dense} and [C I]-CO ratios

The line ratio $R_{[CI]}$ can be used to determine directly the excitation temperature by adopting the equation T_{ex} = 38.8 K/ln[2.11/$R_{[CI]}$] in optically thin limit (Stutzki et al., 1997). The excitation temperatures are typically in the range of 20–30 K for our sample, which is close to the excitation energy of [C I] (1–0) (24 K) but significantly lower than that of [C I] (2–1) (63 K). Tan et al. (2018) present the ratios of $L_{IR}/L'_{HCN\,(4-3)}$ and $L_{IR}/L'_{HCO^+\,(4-3)}$ as a function of color f70/f100 μm for MALATANG galaxies NGC 253, IC 342, and NGC 6946, and find both $L_{IR}/L'_{HCN\,(4-3)}$ and $L_{IR}/L'_{HCO^+\,(4-3)}$ correlate moderate and positive with f70/f100 μm. In the study of Jiao et al. (2017); Jiao et al. (2019), they investigate the dependence of $L'_{[C\ I]\ (1-0)}/L'_{CO\ (1-0)}$, $L'_{[C\ I]\ (2-1)}/L'_{CO\ (1-0)}$ and $R_{[CI]}$ on the color f60/f100μm, and find non-correlation, a weak correlation, and a modest correlation, respectively. The better correlations involving the [C I] (2–1) line ratios with both $L_{IR}/L'_{HCN\,(4-3)}$ and $L_{IR}/L'_{HCO^+\,(4-3)}$ found in Figure 1, S2 are consistence with the results in Tan et al. (2018).

According to Jiao et al. (2019), the $L'_{[CI](2-1)}/L'_{CO(1-0)}$ and $R_{[CI]}$ ratios exhibit a centrally peaked distribution in starburst galaxies. Krips et al. (2016) and Salak et al. (2019) found that the $L'_{[CI](1-0)}/L'_{CO(1-0)}$ ratio tends to be higher in the bright centers of starburst galaxies NGC 253 and NGC 1808, as well as in LIRG IRAS F18293-3413 (Saito et al., 2020), based on well-resolved datasets observed with ALMA. These results indicate that the strong radiation fields in this active star formation regions with high $L_{IR}/L'_{HCN\,(4-3)}$ and $L_{IR}/L'_{HCO^+\,(4-3)}$ can enhance carbon emissions, which is agree with our results in Figure 1, Supplementary Figure S2.

However, we note that the scatters of $L_{IR}/L'_{HCN\,(4-3)}$ and $L_{IR}/L'_{HCO^+\,(4-3)}$ in resolved galaxies of Tan18 are larger than those in global galaxies of the Zhang14 and Imanishi18 samples. When only considering the Tan18 sample, the correlations between

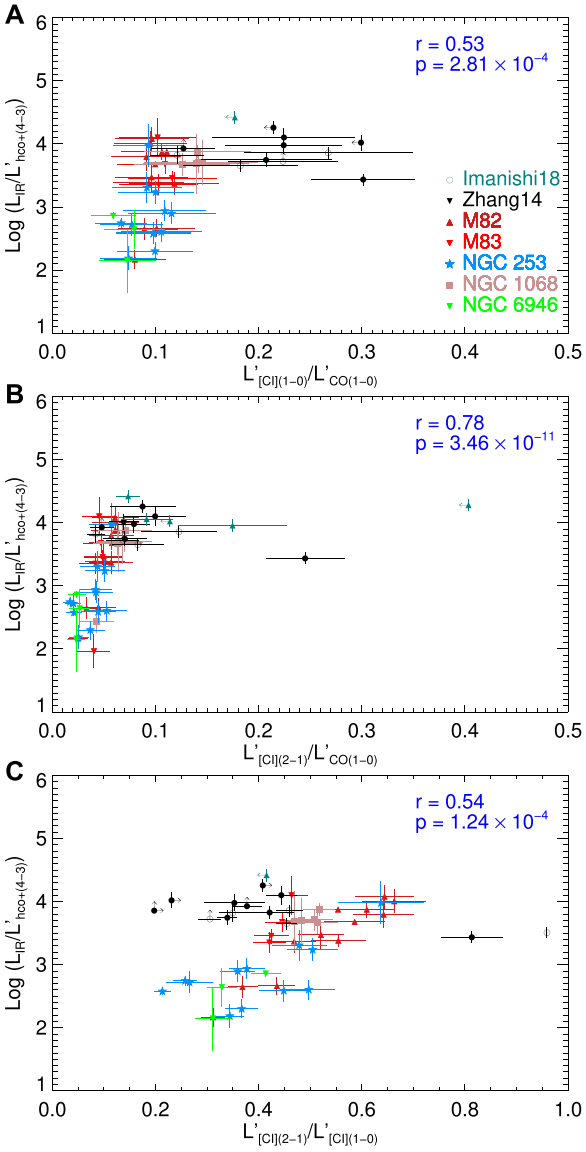

FIGURE 2
Comparison of the luminosity ratios of $L_{IR}/L'_{HCO+(4-3)}$ with the line luminosity ratios of $L'_{[CI]\ (1-0)}/L'_{CO(1-0)}$ **(A)**, $L'_{[CI]\ (2-1)}/L'_{CO(1-0)}$ **(B)**, and $L'_{[CI]\ (2-1)}/L'_{[CI]\ (1-0)}$ **(C)**, respectively. The symbols are same as in Figure 1.

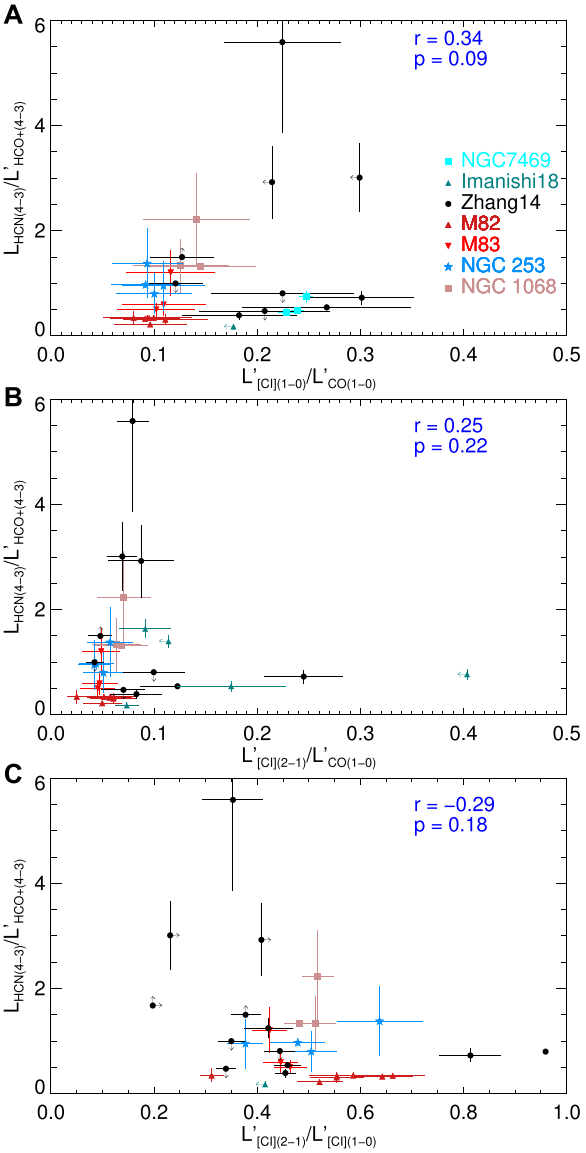

FIGURE 3
Comparison of the line luminosity ratios of $L'_{HCN(4-3)}/L'_{HCO+(4-3)}$ with that of $L'_{[CI]\ (1-0)}/L'_{CO(1-0)}$ **(A)**, $L'_{[CI]\ (2-1)}/L'_{CO(1-0)}$ **(B)**, and $L'_{[CI]\ (2-1)}/L'_{[CI]\ (1-0)}$ **(C)**, respectively. We further add galaxy NGC 7469 adopted from Izumi et al. (2015), Izumi et al. (2020) shown as cyan square, and the other symbols are same as in Figure 1.

$L_{IR}/L'_{HCN(4-3)}$ and $L'_{[C\ I]\ (1-0)}/L'_{CO\ (1-0)}$, $L'_{[C\ I]\ (2-1)}/L'_{CO\ (1-0)}$ and $R_{[CI]}$ are found to be 0.25, 0.66, and 0.78, respectively. Similarly, the correlations between $L_{IR}/L'_{HCO^+\ (4-3)}$ and $L'_{[C\ I]\ (1-0)}/L'_{CO\ (1-0)}$, $L'_{[C\ I]\ (2-1)}/L'_{CO\ (1-0)}$ and $R_{[CI]}$ are 0.46, 0.79, and 0.80 for Tan18 galaxies. However, in the Zhang14 and Imanishi18 samples, both $L_{IR}/L'_{HCN(4-3)}$ and $L_{IR}/L'_{HCO^+\ (4-3)}$ show no significant correlations with the [C I]-CO and $R_{[CI]}$ ratios, with correlation coefficients less than 0.26, except for the relationship between $L_{IR}/L'_{HCO^+\ (4-3)}$ and $R_{[CI]}$. The correlation coefficient for this relationship is −0.41, which is primarily influenced by galaxies NGC 6240 and NGC 4945, in which gas heating is likely dominated by shocks (Wang et al., 2004; Meijerink et al., 2012; Henkel et al., 2018).

The higher correlations observed in resolved samples indicate that $L_{IR}/L'_{HCN(4-3)}$ and $L_{IR}/L'_{HCO^+\ (4-3)}$ may be more sensitive to [C I]-CO and $R_{[CI]}$ ratios in normal SF galaxies than in AGNs, as the Tan18 sample is predominantly composed of SF galaxies, while Zhang14 and Imanishi18 samples are mostly AGNs. This is further supported by the relatively smaller dispersions of $L_{IR}/L'_{HCN(4-3)}$ and $L_{IR}/L'_{HCO^+\ (4-3)}$ in the AGN galaxy NGC 1068 compared to other SF galaxies in Tan18. Additionally, the $L_{IR}/L'_{HCN(4-3)}$ and $L_{IR}/L'_{HCO^+\ (4-3)}$ values are similar to those observed in the Zhang14 and Imanishi18. However, we cannot exclude the possibility that the differences in correlations are due to variations in physical properties between global and resolved regions. Furthermore, variations in

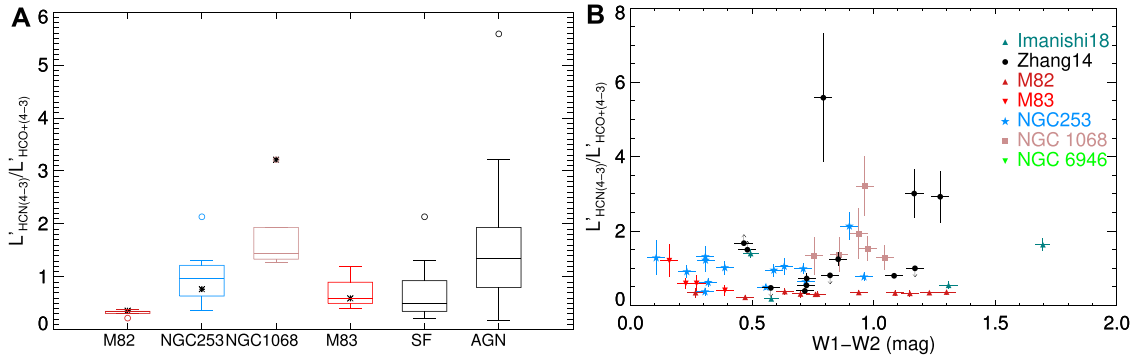

FIGURE 4
(A) boxes show the medians (colored lines in the boxes), the interquartile ranges (colored boxes), and the full range up to 1.5× the interquartile range (IQR; colored horizontal lines) of $L'_{\rm HCN(4-3)}/L'_{\rm HCO+(4-3)}$ for Tan18 sample galaxies, star-forming and AGN systems of whole system. Fliers (points with value >1.5× IQR) are plotted with colored circles, and the central value for Tan18 galaxies are shown as black asterisks. Upper and lower limits are not included in the box plot. **(B)** The $L'_{\rm HCN(4-3)}/L'_{\rm HCO+(4-3)}$ plots against color of W1 - W2 for the sample together.

$L_{\rm IR}/L'_{\rm HCN\,(4-3)}$ and $L_{\rm IR}/L'_{\rm HCO^+\,(4-3)}$ across different regions can be smoothed out when calculating global averages. It should also be noted that the regions detected in HCN (4–3) and HCO^+ (4–3) do not entirely overlap with those observed in [C I] observations, which could potentially introduce some uncertainty to the results.

3.3.2 The variation of $L'_{\rm HCN\,(4-3)}/L'_{\rm HCO^+\,(4-3)}$ ratio

Izumi et al. (2013), Izumi et al. (2015) observed the central kiloparsec region of AGN galaxies of NGC 1097 and NGC 7469 with ALMA at ~ 100 and 150 pc resolutions. Both studies found higher $L'_{\rm HCN\,(4-3)}/L'_{\rm HCO^+\,(4-3)}$ ratios at the nucleus AGN positions than at the starburst rings and starburst galaxies. Compiling data from literature and ALMA archive, including 25 data points for 12 galaxies, Izumi et al. (2016) found that AGNs tend to show higher $L'_{\rm HCN\,(4-3)}/L'_{\rm HCO^+\,(4-3)}$ ratios than starburst galaxies when using only high-resolution samples with spatial resolution < 500 pc, which can differentiate regions energetically dominated by AGNs from those contaminated by coexisting starburst activities. However, when galaxies with low-resolution were superposed, some of the AGNs showed $L'_{\rm HCN\,(4-3)}/L'_{\rm HCO^+\,(4-3)}$ ratios that were comparable to those starburst galaxies. With 35 pc spatial resolution, García-Burillo et al. (2014) reported a globally high $L'_{\rm HCN\,(4-3)}/L'_{\rm HCO^+\,(4-3)}$ ratio in the circumnuclear disk (CND) of NGC 1068, with an average value of ~2.5. Nevertheless, the lowest value of $L'_{\rm HCN\,(4-3)}/L'_{\rm HCO^+\,(4-3)}$ ~1.5 is found precisely at the AGN locus, and a positive gradient up to ~3 is observed in CND regions. Meanwhile, a relatively low $L'_{\rm HCN\,(1-0)}/L'_{\rm HCO^+\,(1-0)}$ ratio in the immediate vicinity of an AGN compared to its CND has also been observed in NGC 1097 (Martín et al., 2015). They reported a value of $L'_{\rm HCN\,(1-0)}/L'_{\rm HCO^+\,(1-0)} = 1.65$ at the AGN position, which reached a maximum value of ~2 in the CND. While both values are higher than the average ratio of ~1.3 calculated in the SF ring.

The $L'_{\rm HCN\,(4-3)}/L'_{\rm HCO^+\,(4-3)}$ ratios in our sample do not show a significant trend between AGN and star-forming galaxies, which is not consistent with the aforementioned results using high resolutions. This inconsistency may be due to the following reasons: (1) The influence of resolution on this line ratio can not be ignored. The effect of AGN can be contaminated and even smoothed out from global average environment when the resolution is not good enough to distinguish AGN from the surrounding SF region. (2) The variation of the line ratio is complex, e.g., it is strongly time-dependent (Meijerink et al., 2013), and easily affected by gas temperature (Viti et al., 2014), molecular chemistry (Izumi et al., 2013; Martín et al., 2015), complicaed opacity (Meier and Turner, 2012), IR pumping by UV/X-ray heated dust (Graciá-Carpio et al., 2006; Matsushita et al., 2015), evolutionary states of activity (Privon et al., 2020), *etc.* Samples with multiple interstellar medium (ISM) conditions may obtain different ratios, however, the study of the physical or chemical influence on the line ratio with models is beyond the scope of our sample discussion. In conclusion, blindly using the line ratio as an AGN indicator without paying attention to resolution can be unreliable.

The ratio of $L'_{\rm HCN\,(4-3)}/L'_{\rm HCO^+\,(4-3)}$ in some SF galaxies, such as NGC 253 and M 83, is comparable to the ratio in AGNs. The higher $L'_{\rm HCN\,(4-3)}/L'_{\rm HCO^+\,(4-3)}$ value observed in NGC 253 may be due to its younger starburst age compared to M 82 (Izumi et al., 2016), which has significantly lower $L'_{\rm HCN\,(4-3)}/L'_{\rm HCO^+\,(4-3)}$ ratios due to the increased fractional abundance of HCO^+ resulting from high ionization effects from cosmic rays in frequent supernovae explosions (Meijerink et al., 2011). However, in NGC 253, the molecular gas heating is likely dominated by shocks (Martín et al., 2006) rather than photodissociation and/or supernovae in M 82. Large velocity gradient (LVG) models with $n_{\rm H_2} = 10^{4.75}$ cm^{-3}, $T_{\rm kin=80\,K}$, and X(HCN) ~ 5X(HCO^+) abundance ratios have been reported for NGC 253 (Meier et al., 2015). The HCN and HCO^+ lines are optically thick and subthermally excited in NGC 253 (Knudsen et al., 2007; Meier et al., 2015), and its dense gas excitations are higher than M 82 and even AGN galaxies of NGC 6240, Mrk 231 via HCN spectral energy distributions (SEDs, Knudsen et al., 2007). Nguyen et al. (1992) reported high $L'_{\rm HCN\,(1-0)}/L'_{\rm HCO^+\,(1-0)} = 1.3$ ratios in M 83, which is even higher than that in NGC 1068.

Using the IRAM 30 m observations of a sample of 58 local luminous and ultraluminous infrared galaxies from the Great Observatories All-sky LIRG Survey, Privon et al. (2015) found that the ratio of $L'_{\rm HCN\,(1-0)}/L'_{\rm HCO+\,(1-0)}$ is higher in AGN-dominated systems compared to composite and starburst-dominated systems. However, the $L'_{\rm HCN\,(1-0)}/L'_{\rm HCO^+\,(1-0)}$ ratios in some composite and starburst systems are comparable to those of AGNs. Therefore, they concluded that enhancement of HCN emission is not uniquely associated with AGNs, which is consistent with our finding in Figure 4. Li et al. (2021) complied a sample with more than 100 galaxies including 70 local galaxies observed with IRAM and samples from Costagliola et al. (2011) and Privon et al. (2015) as well, and found no clear difference of $L'_{\rm HCN\,(1-0)}/L'_{\rm HCO+\,(1-0)}$ ratios between galaxies with or without known AGN activity. Zhou et al. (2022) estimated an average $L'_{\rm HCN\,(2-1)}/L'_{\rm HCO+\,(2-1)}$ ratio of 1.15 ± 0.26 for AGNs, which is only slight higher than that observed in SF galaxies (0.98 ± 0.42). The difference in the ratio is still within 1σ, and thus is not sufficient to separate populations with AGNs. Privon et al. (2020) explored the relationship between $\rm HCN/HCO^+$ ratios for several J levels including $J = 1$–0 and $J = 4$–3 and AGN fractions derived from X-rays, and found no correlations between them. Based on these findings, they concluded that the $\rm HCN/HCO^+$ ratios are not reliable indicators of ongoing supermassive black hole accretion.

4 Summary

In this paper, we select a sample of 26 galaxies which both have dense gas observations of HCN (4–3) and $\rm HCO^+$ (4–3) from Tan et al. (2018); Zhang et al. (2014); Imanishi et al. (2018), and molecular tracers of [C I] and CO observations from Lu et al. (2017); Fernández-Ontiveros et al. (2016); Jiao et al. (2017). We explore the correlations between $L_{\rm IR}/L'_{\rm HCN\,(4-3)}$, $L_{\rm IR}/L'_{\rm HCO^+\,(4-3)}$ and $L'_{\rm [C\ I]\ (1-0)}/L'_{\rm CO\ (1-0)}$, $L'_{\rm [C\ I]\ (2-1)}/L'_{\rm CO\ (1-0)}$ and $R_{\rm [CI]}$. Our findings indicate that $L_{\rm IR}/L'_{\rm HCN\,(4-3)}$ has no significant correlation with $L'_{\rm [C\ I]\ (1-0)}/L'_{\rm CO\ (1-0)}$, but has a modest correlation with both $L'_{\rm [C\ I]\ (2-1)}/L'_{\rm CO\ (1-0)}$ and $R_{\rm [CI]}$. On the other hand, the $L_{\rm IR}/L'_{\rm HCO^+\,(4-3)}$ correlates moderately with all three line luminosity ratios, and the correlations involving the [C I] (2–1) ratios are better than that of $L'_{\rm [C\ I]\ (1-0)}/L'_{\rm CO\ (1-0)}$.

We plot $L'_{\rm HCN\,(4-3)}/L'_{\rm HCO^+\,(4-3)}$ against $L'_{\rm [C\ I]\ (1-0)}/L'_{\rm CO\ (1-0)}$, $L'_{\rm [C\ I]\ (2-1)}/L'_{\rm CO\ (1-0)}$, or $R_{\rm [CI]}$ ratios, and find no obvious correlations for all of them. We present the $L'_{\rm HCN\,(4-3)}/L'_{\rm HCO^+\,(4-3)}$ for AGN and SF galaxies in Tan18, and also plot the $L'_{\rm HCN\,(4-3)}/L'_{\rm HCO^+\,(4-3)}$ with AGN diagnostic of W1 − W2 colors for the total samples. Both show that higher $L'_{\rm HCN\,(4-3)}/L'_{\rm HCO^+\,(4-3)}$ ratios are predominantly found in AGN candidates, while majority of the $L'_{\rm HCN\,(4-3)}/L'_{\rm HCO^+\,(4-3)}$ values in SF galaxies are comparable to those in AGNs, which raises the possibility that $L'_{\rm HCN\,(4-3)}/L'_{\rm HCO^+\,(4-3)}$ may not be a reliable indicator for distinguishing AGN from SF galaxies.

Data availability statement

The raw data supporting the conclusions of this article will be made available by the authors, without undue reservation.

Author contributions

QJ and YuG designed the study, and QJ was the main author of the article. QT and YaG made significant contributions and edits to the text. All authors contributed to the article and approved the submitted version.

Funding

This work is supported by National Natural Science Foundation of China (NSFC, Nos. 12003070 and 12033004). Research Funding of Wuhan Polytechnic University NO. 2022RZ035. Scientific Research Fund of Dezhou University, 3012304024.

Acknowledgments

This research has made use of the NASA/IPAC Infrared Science Archive, which is operated by the Jet Propulsion Laboratory, California Institute of Technology, under contract with the National Aeronautics and Space Administration. This publication makes use of data products from the Wide-field Infrared Survey Explorer, which is a joint project of the University of California, Los Angeles, and the Jet Propulsion Laboratory/California Institute of Technology, and NEOWISE, which is a project of the Jet Propulsion Laboratory/California Institute of Technology. WISE and NEOWISE are funded by the National Aeronautics and Space Administration.

Conflict of interest

The authors declare that the research was conducted in the absence of any commercial or financial relationships that could be construed as a potential conflict of interest.

Publisher's note

Supplementary material

The Supplementary Material for this article can be found online at: https://www.frontiersin.org/articles/10.3389/fspas.2023.1246978/full#supplementary-material

References

Alaghband-Zadeh, S., Chapman, S., Swinbank, A., Smail, I., Danielson, A., Decarli, R., et al. (2013). Using [c i] to probe the interstellar medium in z 2.5 sub-millimeter galaxies. *Mon. Notices R. Astronomical Soc.* 435, 1493–1510. doi:10.1093/mnras/stt1390

Aniano, G., Draine, B. T., Gordon, K., and Sandstrom, K. (2011). Common-resolution convolution kernels for space-and ground-based telescopes. *Publ. Astronomical Soc. Pac.* 123, 1218–1236. doi:10.1086/662219

Baan, W. A., Henkel, C., Loenen, A. F., Baudry, A., and Wiklind, T. (2008). Dense gas in luminous infrared galaxies. *A&A* 477, 747–762. doi:10.1051/0004-6361:20077203

Bertin, E., and Arnouts, S. (1996). Sextractor: software for source extraction. *Astronomy astrophysics Suppl. Ser.* 117, 393–404. doi:10.1051/aas:1996164

Béthermin, M., Greve, T., De Breuck, C., Vieira, J., Aravena, M., Chapman, S., et al. (2018). Dense-gas tracers and carbon isotopes in five 2.5< z< 4 lensed dusty star-forming galaxies from the spt smg sample. *Astronomy Astrophysics* 620, A115. doi:10.1051/0004-6361/201833081

Bigiel, F., Leroy, A. K., Jiménez-Donaire, M. J., Pety, J., Usero, A., Cormier, D., et al. (2016). The EMPIRE survey: systematic variations in the dense gas fraction and star formation efficiency from full-disk mapping of M51. *Astrophysical J. Lett.* 822, L26. doi:10.3847/2041-8205/822/2/l26

Bigiel, F., Leroy, A., Walter, F., Brinks, E., de Blok, W. J. G., Madore, B., et al. (2008). The star formation law in nearby galaxies on sub-kpc scales. *Astronomical J.* 136, 2846–2871. doi:10.1088/0004-6256/136/6/2846

Bisbas, T. G., Papadopoulos, P. P., and Viti, S. (2015). Effective destruction of co by cosmic rays: implications for tracing h2 gas in the universe. *Astrophysical J.* 803, 37. doi:10.1088/0004-637x/803/1/37

Bisbas, T. G., Van Dishoeck, E. F., Papadopoulos, P. P., Szűcs, L., Bialy, S., and Zhang, Z.-Y. (2017). Cosmic-ray induced destruction of co in star-forming galaxies. *Astrophysical J.* 839, 90. doi:10.3847/1538-4357/aa696d

Bolatto, A. D., Wolfire, M., and Leroy, A. K. (2013). The co-to-h2 conversion factor. *Annu. Rev. Astronomy Astrophysics* 51, 207–268. doi:10.1146/annurev-astro-082812-140944

Boogaard, L. A., van der Werf, P., Weiss, A., Popping, G., Decarli, R., Walter, F., et al. (2020). The alma spectroscopic survey in the hubble ultra deep field: co excitation and atomic carbon in star-forming galaxies at z= 1–3. *Astrophysical J.* 902, 109. doi:10.3847/1538-4357/abb82f

Chen, H., Braine, J., Gao, Y., Koda, J., and Gu, Q. (2017). Dense gas in the outer spiral arm of m51. *Astrophysical J.* 836, 101. doi:10.3847/1538-4357/836/1/101

Chen, H., Gao, Y., Braine, J., and Gu, Q. (2015). Spatially resolved dense molecular gas and star formation rate in M51. *Astrophysical J.* 810, 140–149. doi:10.1088/0004-637x/810/2/140

Costagliola, F., Aalto, S., Rodriguez, M., Muller, S., Spoon, H., Martín, S., et al. (2011). Molecules as tracers of galaxy evolution: an EMIR survey: I. Presentation of the data and first results⋆. *Astronomy Astrophysics* 528, A30. doi:10.1051/0004-6361/201015628

Daddi, E., Elbaz, D., Walter, F., Bournaud, F., Salmi, F., Carilli, C., et al. (2010). Different star formation laws for disks versus starbursts at low and high redshifts. *Astrophysical J. Lett.* 714, L118–L122. doi:10.1088/2041-8205/714/1/l118

Dasyra, K., and Combes, F. (2011). Turbulent and fast motions of h2 gas in active galactic nuclei. *Astronomy Astrophysics* 533, L10. doi:10.1051/0004-6361/201117730

Dunne, L., Maddox, S., Papadopoulos, P., Ivison, R., and Gomez, H. (2022). Dust, co, and [c i]: cross-calibration of molecular gas mass tracers in metal-rich galaxies across cosmic time. *Mon. Notices R. Astronomical Soc.* 517, 962–999. doi:10.1093/mnras/stac2098

Evans, N. J., Heiderman, A., Vutisalchavakul, N., et al. (2014). Star formation relations in nearby molecular clouds. *Astrophysical J.* 782, 114. doi:10.1088/0004-637x/782/2/114

Fernández-Ontiveros, J. A., Spinoglio, L., Pereira-Santaella, M., Malkan, M. A., Andreani, P., and Dasyra, K. M. (2016). Far-infrared line spectra of active galaxies from the herschel/pacs spectrometer: the complete database. *Astrophysical J. Suppl. Ser.* 226, 19. doi:10.3847/0067-0049/226/2/19

Gaches, B. A., Offner, S. S., and Bisbas, T. G. (2019). The astrochemical impact of cosmic rays in protoclusters. ii. ci-to-h2 and co-to-h2 conversion factors. *Astrophysical J.* 883, 190. doi:10.3847/1538-4357/ab3c5c

Galametz, M., Kennicutt, R., Calzetti, D., Aniano, G., Draine, B. T., Boquien, M., et al. (2013). Calibration of the total infrared luminosity of nearby galaxies from spitzer and herschel bands. *Mon. Notices R. Astronomical Soc.* 431, 1956–1986. doi:10.1093/mnras/stt313

Gao, Y., Carilli, C. L., Solomon, P. M., and Bout, P. A. V. (2007). Hcn observations of dense star-forming gas in high-redshift galaxies. *Astrophysical J. Lett.* 660, L93–L96. doi:10.1086/518244

Gao, Y., and Solomon, P. M. (2004a). HCN survey of normal spiral, infrared-luminous, and ultraluminous galaxies. *Astrophysical J. Suppl. Ser.* 152, 63–80. doi:10.1086/383003

Gao, Y., and Solomon, P. M. (2004b). The star formation rate and dense molecular gas in galaxies. *Astrophysical J.* 606, 271–290. doi:10.1086/382999

García-Burillo, S., Combes, F., Usero, A., Aalto, S., Krips, M., Viti, S., et al. (2014). Molecular line emission in ngc 1068 imaged with alma-i. an agn-driven outflow in the dense molecular gas. *Astronomy Astrophysics* 567, A125. doi:10.1051/0004-6361/201423843

García-Burillo, S., Usero, A., Alonso-Herrero, A., Graciá-Carpio, J., Pereira-Santaella, M., Colina, L., et al. (2012). Star-formation laws in luminous infrared galaxies: new observational constraints on models⋆. *Astronomy Astrophysics* 539, A8. doi:10.1051/0004-6361/201117838

Glover, S. C., and Clark, P. C. (2016). Is atomic carbon a good tracer of molecular gas in metal-poor galaxies? *Mon. Notices R. Astronomical Soc.* 456, 3596–3609. doi:10.1093/mnras/stv2863

Glover, S. C., Clark, P. C., Micic, M., and Molina, F. (2015). Modelling [c i] emission from turbulent molecular clouds. *Mon. Notices R. Astronomical Soc.* 448, 1607–1627. doi:10.1093/mnras/stu2699

Graciá-Carpio, J., García-Burillo, S., Planesas, P., and Colina, L. (2006). Is hcn a true tracer of dense molecular gas in luminous and ultraluminous infrared galaxies? *Astrophysical J.* 640, L135–L138. doi:10.1086/503361

Graciá-Carpio, J., García-Burillo, S., Planesas, P., Fuente, A., and Usero, A. (2008). Evidence of enhanced star formation efficiency in luminous and ultraluminous infrared galaxies. *Astronomy Astrophysics* 479, 703–717. doi:10.1051/0004-6361:20078223

Henkel, C., Mühle, S., Bendo, G., Józsa, G., Gong, Y., Viti, S., et al. (2018). Molecular line emission in ngc 4945, imaged with alma. *Astronomy Astrophysics* 615, A155. doi:10.1051/0004-6361/201732174

Ikeda, M., Maezawa, H., Ito, T., Saito, G., Sekimoto, Y., Yamamoto, S., et al. (1999). Large-scale mapping observations of the C [CSC]i[/CSC] ([TSUP]3[/TSUP] [ital]P[/ITAL] [TINF]1[/TINF]–[TSUP]3[/TSUP] [ital]P[/ITAL] [TINF]0[/TINF]) and CO ([ITAL]J[/ITAL] = 3–2) lines toward the orion A molecular cloud. *Astrophysical J.* 527, L59–L62. doi:10.1086/312395

Ikeda, M., Oka, T., Tatematsu, K., Sekimoto, Y., and Yamamoto, S. (2002). The distribution of atomic carbon in the orion giant molecular cloud 1. *Astrophysical J. Suppl. Ser.* 139, 467–485. doi:10.1086/338761

Imanishi, M., Nakanishi, K., and Izumi, T. (2018). Alma multiple-transition observations of high-density molecular tracers in ultraluminous infrared galaxies. *Astrophysical J.* 856, 143. doi:10.3847/1538-4357/aab42f

Israel, F., Rosenberg, M., and van der Werf, P. (2015). Neutral carbon and co in 76 (u) lirgs and starburst galaxy centers-a method to determine molecular gas properties in luminous galaxies. *Astronomy Astrophysics* 578, A95. doi:10.1051/0004-6361/201425175

Izumi, T., Kohno, K., Aalto, S., Doi, A., Espada, D., Fathi, K., et al. (2015). Alma observations of the submillimeter dense molecular gas tracers in the luminous type-1 active nucleus of ngc 7469. *Astrophysical J.* 811, 39. doi:10.1088/0004-637x/811/1/39

Izumi, T., Kohno, K., Aalto, S., Espada, D., Fathi, K., Harada, N., et al. (2016). Submillimeter-hcn diagram for energy diagnostics in the centers of galaxies. *Astrophysical J.* 818, 42. doi:10.3847/0004-637x/818/1/42

Izumi, T., Kohno, K., Martín, S., Espada, D., Harada, N., Matsushita, S., et al. (2013). Submillimeter ALMA observations of the dense gas in the low-luminosity type-1 active nucleus of NGC1097. *Publ. Astron. Soc. Jpn. Nihon. Tenmon. Gakkai.* 65, 100. doi:10.1093/pasj/65.5.100

Izumi, T., Nguyen, D. D., Imanishi, M., Kawamuro, T., Baba, S., Nakano, S., et al. (2020). Alma observations of multiple co and c lines toward the active galactic nucleus of ngc 7469: an x-ray-dominated region caught in the act. *Astrophysical J.* 898, 75. doi:10.3847/1538-4357/ab9cb1

Jiang, X.-J., Greve, T. R., Gao, Y., Zhang, Z.-Y., Tan, Q., de Grijs, R., et al. (2020). The MALATANG survey: dense gas and star formation from high-transition HCN and HCO+ maps of NGC 253. *Mon. Notices R. Astronomical Soc.* 494, 1276–1296. doi:10.1093/mnras/staa794

Jiao, Q., Zhao, Y., Lu, N., Gao, Y., Salak, D., Zhu, M., et al. (2019). Resolved neutral carbon emission in nearby galaxies:[c i] lines as total molecular gas tracers. *Astrophysical J.* 880, 133. doi:10.3847/1538-4357/ab29ed

Jiao, Q., Zhao, Y., Zhu, M., Lu, N., Gao, Y., and Zhang, Z.-Y. (2017). Neutral carbon emission in luminous infrared galaxies: the [c i] lines as total molecular gas tracers. *Astrophysical J. Lett.* 840, L18. doi:10.3847/2041-8213/aa6f0f

Jiménez-Donaire, M. J., Bigiel, F., Leroy, A., Usero, A., Cormier, D., Puschnig, J., et al. (2019). Empire: the iram 30 m dense gas survey of nearby galaxies. *Astrophysical J.* 880, 127. doi:10.3847/1538-4357/ab2b95

Kamenetzky, J., Rangwala, N., Glenn, J., Maloney, P., and Conley, A. (2016). Relations with co rotational ladders of galaxies across the herschel spire archive. *Astrophysical J.* 829, 93. doi:10.3847/0004-637x/829/2/93

Kennicutt, J. R. C., and Evans, N. J. (2012). Star formation in the milky way and nearby galaxies. *Annu. Rev. Astronomy Astrophysics* 50, 531–608. doi:10.1146/annurev-astro-081811-125610

Kennicutt, R. C. J. (1998). The global schmidt law in star-forming galaxies. *Astrophysical J.* 498, 541–552. doi:10.1086/305588

Knudsen, K., Walter, F., Weiss, A., Bolatto, A., Riechers, D., and Menten, K. (2007). New insights on the dense molecular gas in ngc 253 as traced by hcn and hco+. *Astrophysical J.* 666, 156–164. doi:10.1086/519761

Krips, M., Martín, S., Sakamoto, K., Aalto, S., Bisbas, T., Bolatto, A., et al. (2016). Aca [ci] observations of the starburst galaxy ngc 253. *Astronomy Astrophysics* 592, L3. doi:10.1051/0004-6361/201628882

Krips, M., Neri, R., García-Burillo, S., Martín, S., Combes, F., Graciá-Carpio, J., et al. (2008). A multi-transition hcn and hco+ study of 12 nearby active galaxies: active galactic nucleus versus starburst environments. *Astrophysical J.* 677, 262–275. doi:10.1086/527367

Kuno, N., Sato, N., Nakanishi, H., Hirota, A., Tosaki, T., Shioya, Y., et al. (2007). Nobeyama co atlas of nearby spiral galaxies: distribution of molecular gas in barred and nonbarred spiral galaxies. *Publ. Astronomical Soc. Jpn.* 59, 117–166. doi:10.1093/pasj/59.1.117

Lada, C. J., Forbrich, J., Lombardi, M., and Alves, J. F. (2012). Star formation rates in molecular clouds and the nature of the extragalactic scaling relations. *Astrophysical J.* 745, 190. doi:10.1088/0004-637x/745/2/190

Lada, C. J., Lombardi, M., and Alves, J. F. (2010). On the star formation rates in molecular clouds. *Astrophysical J.* 724, 687–693. doi:10.1088/0004-637x/724/1/687

Lee, M. M., Tanaka, I., Iono, D., Kawabe, R., Kodama, T., Kohno, K., et al. (2021). Revisited cold gas content with atomic carbon [c i] in z= 2.5 protocluster galaxies. *Astrophysical J.* 909, 181. doi:10.3847/1538-4357/abdbb5

Li, F., Wang, J., Fang, M., Tan, Q.-H., Zhang, Z.-Y., Gao, Y., et al. (2020). Hcn 3–2 survey towards a sample of local galaxies. *Publ. Astronomical Soc. Jpn.* 72, 41. doi:10.1093/pasj/psaa025

Li, F., Wang, J., Gao, F., Liu, S., Zhang, Z.-Y., Li, S., et al. (2021). Dense gas in local galaxies revealed by multiple tracers. *Mon. Notices R. Astronomical Soc.* 503, 4508–4528. doi:10.1093/mnras/stab745

Liu, D., Gao, Y., Isaak, K., Daddi, E., Yang, C., Lu, N., et al. (2015). High-j co versus far-infrared relations in normal and starburst galaxies. *Astrophysical J. Lett.* 810, L14. doi:10.1088/2041-8205/810/2/l14

Liu, T., Kim, K.-T., Yoo, H., Liu, S.-y., Tatematsu, K., Qin, S.-L., et al. (2016). Star formation laws in both galactic massive clumps and external galaxies: extensive study with dust coninuum, hcn (4-3), and cs (7-6). *Astrophysical J.* 829, 59. doi:10.3847/0004-637x/829/2/59

Lu, N., Zhao, Y., Díaz-Santos, T., Xu, C. K., Gao, Y., Armus, L., et al. (2017). A herschel space observatory spectral line survey of local luminous infrared galaxies from 194 to 671 microns. *Astrophysical J. Suppl. Ser.* 230, 1. doi:10.3847/1538-4365/aa6476

Makiwa, G., Naylor, D. A., Ferlet, M., Salji, C., Swinyard, B., Polehampton, E., et al. (2013). Beam profile for the herschel–spire fourier transform spectrometer. *Appl. Opt.* 52, 3864–3875. doi:10.1364/ao.52.003864

Martín, S., Kohno, K., Izumi, T., Krips, M., Meier, D., Aladro, R., et al. (2015). Multimolecule alma observations toward the seyfert 1 galaxy ngc 1097. *Astronomy Astrophysics* 573, A116. doi:10.1051/0004-6361/201425105

Martín, S., Mauersberger, R., Martín-Pintado, J., Henkel, C., and García-Burillo, S. (2006). A 2 millimeter spectral line survey of the starburst galaxy ngc 253. *Astrophysical J. Suppl. Ser.* 164, 450–476. doi:10.1086/503297

Matsushita, S., Boone, F., Krips, M., Lim, J., Muller, S., et al. (2015). Resolving the bright hcn (1- 0) emission toward the seyfert 2 nucleus of m51: shock enhancement by radio jets and weak masing by infrared pumping? *Astrophysical J.* 799, 26. doi:10.1088/0004-637x/799/1/26

Meier, D. S., and Turner, J. L. (2012). Spatially resolved chemistry in nearby galaxies. ii. the nuclear bar in maffei 2. *Astrophysical J.* 755, 104. doi:10.1088/0004-637x/755/2/104

Meier, D. S., Walter, F., Bolatto, A. D., Leroy, A. K., Ott, J., Rosolowsky, E., et al. (2015). Alma multi-line imaging of the nearby starburst ngc 253. *Astrophysical J.* 801, 63. doi:10.1088/0004-637x/801/1/63

Meijerink, R., Kristensen, L., Weiß, A., Van der Werf, P., Walter, F., Spaans, M., et al. (2012). Evidence for co shock excitation in ngc 6240 from herschel spire spectroscopy. *Astrophysical J. Lett.* 762, L16. doi:10.1088/2041-8205/762/2/l16

Meijerink, R., and Spaans, M. (2005). Diagnostics of irradiated gas in galaxy nuclei-i. a far-ultraviolet and x-ray dominated region code. *Astronomy Astrophysics* 436, 397–409. doi:10.1051/0004-6361:20042398

Meijerink, R., Spaans, M., and Israel, F. (2007). Diagnostics of irradiated dense gas in galaxy nuclei-ii. a grid of xdr and pdr models. *Astronomy Astrophysics* 461, 793–811. doi:10.1051/0004-6361:20066130

Meijerink, R., Spaans, M., Kamp, I., Aresu, G., Thi, W.-F., and Woitke, P. (2013). Tracing the physical conditions in active galactic nuclei with time-dependent chemistry. *J. Phys. Chem. A* 117, 9593–9604. doi:10.1021/jp312289f

Meijerink, R., Spaans, M., Loenen, A., and van der Werf, P. P. (2011). Star formation in extreme environments: the effects of cosmic rays and mechanical heating. *Astronomy Astrophysics* 525, A119. doi:10.1051/0004-6361/201015136

Mirabel, I., Booth, R., Garay, G., Johansson, L., and Sanders, D. (1990). Co (1-0) emission from luminous infrared galaxies in the southern hemisphere. *Astronomy Astrophysics* 236, 327–332.

Nguyen, Q., Jackson, J. M., Henkel, C., Truong, B., Mauersberger, R., et al. (1992). A survey for extragalactic hcn and hco (+). *Astrophysical J.* 399, 521–532. doi:10.1086/171944

Offner, S. S., Bisbas, T. G., Bell, T. A., and Viti, S. (2014). An alternative accurate tracer of molecular clouds: the 'x ci-factor. *Mon. Notices R. Astronomical Soc. Lett.* 440, L81–L85. doi:10.1093/mnrasl/slu013

Oteo, I., Zhang, Z., Yang, C., Ivison, R., Omont, A., Bremer, M., et al. (2017). High dense gas fraction in intensely star-forming dusty galaxies. *Astrophysical J.* 850, 170. doi:10.3847/1538-4357/aa8ee3

Papadopoulos, P., Dunne, L., and Maddox, S. (2022). The subthermal excitation of the c i lines in the molecular gas reservoirs of galaxies: its significance and potential utility. *Mon. Notices R. Astronomical Soc.* 510, 725–733. doi:10.1093/mnras/stab3194

Papadopoulos, P. P., Bisbas, T. G., and Zhang, Z.-Y. (2018). New places and phases of co-poor/c i-rich molecular gas in the universe. *Mon. Notices R. Astronomical Soc.* 478, 1716–1725. doi:10.1093/mnras/sty1077

Papadopoulos, P. P., and Greve, T. R. (2004). Ci emission in ultraluminous infrared galaxies as a molecular gas mass tracer. *Astrophysical J.* 615, L29–L32. doi:10.1086/426059

Papadopoulos, P. P., Thi, W.-F., and Viti, S. (2004). C i lines as tracers of molecular gas, and their prospects at high redshifts. *Mon. Notices R. Astronomical Soc.* 351, 147–160. doi:10.1111/j.1365-2966.2004.07762.x

Papadopoulos, P. P., van der Werf, P. P., Xilouris, E., Isaak, K. G., Gao, Y., and Mühle, S. (2012). The molecular gas in luminous infrared galaxies–i. co lines, extreme physical conditions and their drivers. *Mon. Notices R. Astronomical Soc.* 426, 2601–2629. doi:10.1111/j.1365-2966.2012.21001.x

Popping, G., Decarli, R., Man, A. W., Nelson, E. J., Béthermin, M., De Breuck, C., et al. (2017). ALMA reveals starburst-like interstellar medium conditions in a compact star-forming galaxy atz~ 2 using [CI] and CO. *Astronomy Astrophysics* 602, A11. doi:10.1051/0004-6361/201730391

Privon, G. C., Ricci, C., Aalto, S., Viti, S., Armus, L., Diaz-Santos, T., et al. (2020). A hard x-ray test of hcn enhancements as a tracer of embedded black hole growth. *Astrophysical J.* 893, 149. doi:10.3847/1538-4357/ab8015

Privon, G., Herrero-Illana, R., Evans, A., Iwasawa, K., Perez-Torres, M., Armus, L., et al. (2015). Excitation mechanisms for hcn (1–0) and hco+ (1–0) in galaxies from the great observatories all-sky lirg survey. *Astrophysical J.* 814, 39. doi:10.1088/0004-637x/814/1/39

Reiter, M., Shirley, Y. L., Wu, J., Brogan, C., Wootten, A., and Tatematsu, K. (2011). The physical properties of high-mass star-forming clumps: A systematic comparison of molecular tracers. *Astrophysical J. Suppl. Ser.* 195, 1. doi:10.1088/0067-0049/195/1/1

Saito, T., Michiyama, T., Liu, D., Ao, Y., Iono, D., Nakanishi, K., et al. (2020). The 300-pc scale alma view of [c i] 3 p 1–3 p 0, co j= 1–0, and 609-μ m dust continuum in a luminous infrared galaxy. *Mon. Notices R. Astronomical Soc.* 497, 3591–3600. doi:10.1093/mnras/staa2086

Salak, D., Nakai, N., Miyamoto, Y., Yamauchi, A., and Tsuru, T. G. (2013). Large-field co (j= 1 0) observations of the starburst galaxy m 82. *Publ. Astronomical Soc. Jpn.* 65, 66. doi:10.1093/pasj/65.3.66

Salak, D., Nakai, N., Seta, M., and Miyamoto, Y. (2019). Alma observations of atomic carbon [c i](3p1 3p0) and low-j co lines in the starburst galaxy ngc 1808. *Astrophysical J.* 887, 143. doi:10.3847/1538-4357/ab55dc

Sanders, D., Mazzarella, J., Kim, D.-C., Surace, J., and Soifer, B. (2003). The iras revised bright galaxy sample. *Astronomical J.* 126, 1607–1664. doi:10.1086/376841

Sanders, D., Scoville, N., and Soifer, B. (1991). Molecular gas in luminous infrared galaxies. *Astrophysical J.* 370, 158–171. doi:10.1086/169800

Shimajiri, Y., André, P., Braine, J., Könyves, V., Schneider, N., Bontemps, S., et al. (2017). Testing the universality of the star-formation efficiency in dense molecular gas. *Astronomy Astrophysics* 604, A74. doi:10.1051/0004-6361/201730633

Shimajiri, Y., Sakai, T., Tsukagoshi, T., Kitamura, Y., Momose, M., Saito, M., et al. (2013). Extensive [c i] mapping toward the orion-a giant molecular cloud. *Astrophysical J. Lett.* 774, L20. doi:10.1088/2041-8205/774/2/l20

Soifer, B., Neugebauer, G., Matthews, K., Egami, E., Becklin, E., Weinberger, A., et al. (2000). High resolution mid-infrared imaging of ultraluminous infrared galaxies. *Astronomical J.* 119, 509–523. doi:10.1086/301233

Solomon, P., Downes, D., Radford, S., and Barrett, J. (1997). The molecular interstellar medium in ultraluminous infrared galaxies. *Astrophysical J.* 478, 144–161. doi:10.1086/303765

Solomon, P., Downes, D., and Radford, S. (1992). Dense molecular gas and starbursts in ultraluminous galaxies. *Astrophysical J.* 387, L55–L59. doi:10.1086/186304

Stern, D., Assef, R. J., Benford, D. J., Blain, A., Cutri, R., Dey, A., et al. (2012). *Mid-infrared selection of agn with the wide-field infrared survey explorer. i. characterizing wise-selected agn in cosmos*. arXiv preprint arXiv:1205.0811.

Stutzki, J., Graf, U., Haas, S., Honingh, C., Hottgenroth, D., Jacobs, K., et al. (1997). Atomic carbon in M82: physical conditions derived from simultaneous observations of the [C [CSC]i[/CSC]] fine-structure submillimeter-wave transitions. *Astrophysical J.* 477, L33–L36. doi:10.1086/310514

Tan, Q.-H., Gao, Y., Zhang, Z.-Y., Greve, T. R., Jiang, X.-J., Wilson, C. D., et al. (2018). The malatang survey: the l gas–l ir correlation on sub-kiloparsec scale in six nearby star-forming galaxies as traced by hcn j= 4 3 and hco+ j= 4 3. *Astrophysical J.* 860, 165. doi:10.3847/1538-4357/aac512

Usero, A., Leroy, A. K., Walter, F., Schruba, A., García-Burillo, S., Sandstrom, K., et al. (2015). Variations in the star formation efficiency of the dense molecular gas across the disks of star-forming galaxies. *Astronomical J.* 150, 115. doi:10.1088/0004-6256/150/4/115

Valentino, F., Magdis, G. E., Daddi, E., Liu, D., Aravena, M., Bournaud, F., et al. (2018). A survey of atomic carbon [c i] in high-redshift main-sequence galaxies. *Astrophysical J.* 869, 27. doi:10.3847/1538-4357/aaeb88

Valentino, F., Magdis, G. E., Daddi, E., Liu, D., Aravena, M., Bournaud, F., et al. (2020). The properties of the interstellar medium of galaxies across time as traced by the neutral atomic carbon [c i]. *Astrophysical J.* 890, 24. doi:10.3847/1538-4357/ab6603

Viti, S., García-Burillo, S., Fuente, A., Hunt, L., Usero, A., Henkel, C., et al. (2014). Molecular line emission in NGC 1068 imaged with ALMA: II. The chemistry of the dense molecular gas⋆. *Astronomy Astrophysics* 570, A28. doi:10.1051/0004-6361/201424116

Wang, M., Henkel, C., Chin, Y.-N., Whiteoak, J., Cunningham, M. H., Mauersberger, R., et al. (2004). Dense gas in nearby galaxies: XVI. The nuclear starburst environment in NGC 4945. *Astronomy Astrophysics* 422, 883–905. doi:10.1051/0004-6361:20035722

Weiß, A., Downes, D., Henkel, C., and Walter, F. (2005). Atomic carbon at redshift ~2.5. *Astronomy Astrophysics* 429, L25–L28. doi:10.1051/0004-6361:200400085

Weiß, A., Henkel, C., Downes, D., and Walter, F. (2003). Gas and dust in the cloverleaf quasar at redshift 2.5. *Astronomy Astrophysics* 409, L41–L45. doi:10.1051/0004-6361:20031337

Wu, J., Evans, N. J. I., Gao, Y., Solomon, P. M., Shirley, Y. L., and Vanden Bout, P. A. (2005). Connecting dense gas tracers of star formation in our galaxy to high-z star formation. *Astrophysical J.* 635, L173–L176. doi:10.1086/499623

Wu, J., Evans, N. J., II, Shirley, Y. L., and Knez, C. (2010). The properties of massive, dense clumps: mapping surveys of hcn and cs. *Astrophysical J. Suppl. Ser.* 188, 313–357. doi:10.1088/0067-0049/188/2/313

Yang, C., Omont, A., Beelen, A., Gao, Y., van Der Werf, P., Gavazzi, R., et al. (2017). Molecular gas in the*Herschel*-selected strongly lensed submillimeter galaxies atz ∼ 2–4 as probed by multi-*J*CO lines. *Astronomy Astrophysics* 608, A144. doi:10.1051/0004-6361/201731391

Zhang, Z.-Y., Gao, Y., Henkel, C., Zhao, Y., Wang, J., Menten, K. M., et al. (2014). Dense gas tracers and star formation laws in active galaxies: apex survey of hcn j= 4 3, hco+ j= 4 3, and cs j= 7 6. *Astrophysical J. Lett.* 784, L31. doi:10.1088/2041-8205/784/2/l31

Zhou, J., Zhang, Z.-Y., Gao, Y., Wang, J., Shi, Y., Gu, Q., et al. (2022). Dense gas and star formation in nearby infrared-bright galaxies: apex survey of hcn and hco+ j= 2 1. *Astrophysical J.* 936, 58. doi:10.3847/1538-4357/ac82eb